POSTERS

1. **Incidental Detection of Gastric GIST on PSMA PET**
   Jiaqiong Wang; Jian Q Yu
2. **Pseudo-Degenerative Uptake: A Nuclear Medicine Pitfall**
   Eduardo Sanchez-Perez, MD; Ana Y. Valdivia, MD
3. **Hyperkinetic Gallbladder on HIDA Scan: Clinical Outcomes in a Case Series of Patients with Elevated Gallbladder Ejection Fraction**
   Siddarth Ragupathi, MD; Alireza Mohseni, MD; Kwang J. Chun, MD; Renee M. Moadel, MD; Syed Mahmood, MD
4. **Interictal 18F-FDG-PET Hypometabolism concordance with EEG, MRI and Clinical Outcomes in Patients with Epilepsy**
   Affaf Gul, MD; Shazia Naseem, MD; Renee M. Moadel, MD; Syed Mahmood, MD
5. **SUV Max and Tumor Staging in Screening-Detected Lung Cancers: Findings from a Community Program**
   Kevin Hricko BA MS MPH; Louis Mazzarelli MD; Karen Geary; Alexander Mazzarelli; Richard G. Barr MD
6. **Diagnostic Value of Routine Delayed Pelvic Imaging in ^{68}Ga-PSMA PET/CT for Patients with Early Biochemical Recurrence of Prostate Cancer**
   Karen Jia; Jonathan Kuten; Josef Fox; Heiko Schoder; Ali Aria Razmaria
7. **Brain SPECT/CT With Acetazolamide (Diamox) in Management of Patients With Moyamoya Disease**
   Zahra Karimi, MD; Affaf Gul, MD; Siddarth Ragupathi, MD; Kwang J Chun, MD; Ana Valdivia, MD
8. **Preventing Errors in Administered Radiopharmaceutical Doses in Nuclear Medicine**
   Ghazaleh Mehdipour, MD; Kwang J. Chun, MD
9. **Unexpected PSMA Uptake within the Spleen: A Case Report and Review of the Literature**
   Stephen J. Sozio, DO, MBS; William Y. Raynor, MD; Levi Sokol, MD; Dhruv Patel, MD; Jeffrey S. Kempf, MD, FACR
10. **Concordance Between Visual Interpretation and Centiloid Quantification of Amyloid PET/CT in a Retrospective Quality Improvement Study**
    William Y. Raynor, MD; Andrew Soliman, MD; Levi Sokol, MD; Jeffrey S. Kempf, MD, FACR
11. **18F-Florbetapir Amyloid PET Quantification Remains Stable with Shorter Acquisition Times**
    Alfredo Lucas; Rebecca Ward; Safiya I. Lahlaf; Jacob Dubroff; Austin Pantel; Ilya Nasrallah; Philipose G. Mulugeta
12. **Multifocal FDG-Avid Osseous Sarcoidosis on PET/CT: An Interesting Case Presentation**
    Nicholas Campo, MD; William Y. Raynor, MD; Stephen J. Sozio, DO, MBS; Levi Sokol, MD; Anthony Yudd MD, PhD, FACR; Jeffrey Kempf MD, FACR
13. **Toward a Virtual Biopsy for Indeterminate Renal Masses: Multiparametric Contrast-Enhanced Ultrasound and Tc-99m Sestamibi SPECT Case Series**
    Louis Mazzarelli MD; Kevin Hricko MS MPH; Joseph Brito MD; Timothy Tran MD; Alexander Mazzarelli; Richard G. Barr MD
14. **Lymphoscintigraphic Evaluation of Postoperative Lymphocele: Educational Insights from a Case Study**
    Alireza Mohseni; Shazia Naseem; Siddarth Ragupathi; Kwang Chun; Ana Valdivia
15. **Implementing Post-Therapy PSMA Imaging in a Multidisciplinary Theranostics Clinic**
    Nina Le, MD; Christopher Caravella, LNMT; Baho Sidiqi, MD; Clary Evans, MD; Josephine Rini, MD

16. **From Suspicion to Stratification: PET/CT in Pediatric Langerhans Cell Histiocytosis Disease Characterization**
    Graeme Benzie, MD, MSc; Aram Tonoyan, MD, PhD; Tae-young Roh, BSc; Prasanta Karak, MD
17. **Expanding Applications of PET/CT in Pediatrics: From Oncology to Neurology**
    Muhammad Awais Ashraf, D.O.; Veronica Pereira, M.D.; Prasanta Karak, M.D.
18. **Diagnostic Pitfalls of Cardiac FDG PET/CT in Sarcoidosis: Influence of Inadequate Myocardial Suppression Protocols**
    Shazia Naseem, MD; Affaf Gul, MD; Alireza Mohseni MD; Syed Mahmood, MD
19. **FDG-PET/CT: A Cornerstone in Diagnosing and Managing Pyogenic Spondylodiscitis - Vertebral Osteomyelitis**
    Aram Tonoyan, MD, PhD; Graeme Benzie, MD, MSc; Prasanta Karak, MD
20. **Facilitating Artificial Intelligence Education in Nuclear Medicine: Assessing Needs, Perceptions, and Curricular Gaps**
    Shazia Naseem, MD; Affaf Gul, MD; Renee M. Moadel, MD; Syed Mahmood, MD
21. **Development and Validation of the Nonuniform Intense Bowel Uptake (NIBU) Score: A Standardized Semi-Quantitative Tool for Assessing FDG Intense Bowel Uptake Heterogeneity on PET/CT**
    Eduardo A. Sanchez-Perez, MD; Syed Mahmood, MD; Ana Valdivia, MD
22. **FDG PET/CT Lights the Way: When Conventional Imaging Falters in Suspected Infection and Inflammation**
    Muhammad Awais Ashraf, D.O.; Veronica Pereira, M.D.; Racquel Helsing, M.D; Prasanta Karak, M.D
23. **Optimization of a Numerical Observer for Use in Reconstructed Pediatric SPECT Kidney Images**
    Sarah Van Hoesen; Dr. Ted Treves; Dr. Michael King; Dr. William McCarthy
24. **Signs in Brain Death Scintigraphy: the Good, the Bad and the Useless**
    Lionel S. Zuckier, MD
25. **Primary Hepatocellular Carcinoma Incidentally Detected on PSMA PET/CT**
    Kush Patel, MD; William Y. Raynor, MD; Samar Hajj, MD; Anupriya Barot, MD; Don Goldstein, MD; Rizvan Azimzade, MD; Stephen Sozio, DO; Jeffrey S. Kempf, MD, FACR
26. **Added Value of Brain [68Ga]-DOTATATE PET/CT and PET/MRI in Assessing Internal Auditory Canal Involvement in Skull Base Meningioma**
    Preeti Kakkar; Valentina Marulanda Corzo; Kellen Vo Vu; Rajiv S. Magge; Andrew Brandmaier; Joseph R. Osborne; Jana Ivanidze
27. **PSMA PET/CT Studies at Time of Suspected Recurrence of Prostate Cancer in Patients Post Radical Prostatectomy**
    Jaun Young-Johnson, BA; Yi Li, MD; Simin Dadparvar, MD
28. **Diagnosis, Please! Test Your Radiologic Reasoning**
    Veronica Pereira, M.D.; Muhammad Awais Ashraf, D.O.; Prasanta Karak, M.D.

Incidental Detection of Gastric GIST on PSMA PET

Jiaqiong Wang, Jian Q Yu

Jiaqiong Wang, MD, PhD, Assistant Professor, Division of Nuclear Medicine, Department of Radiology, Temple University Health System, Fox Chase Cancer Center, Philadelphia, PA 19140, USA. Email: Jiaqiong.Wang@tuhs.temple.edu

Jian Q Yu, MD, Professor, Division of Nuclear Medicine, Department of Radiology, Temple University Health System, Fox Chase Cancer Center, Philadelphia, PA 19111, USA. Email: Michael.Yu@fccc.edu

Abstract:

Background: In addition to prostate cancer, prostate-specific membrane antigen (PSMA) is expressed in the neovasculature of various other tumor. As early as 2009, immunohistochemistry studies have detected PSMA expression in the neovasculature of gastric and colorectal carcinomas and liver metastasis (Haffner et al., 2009). Case reports have also described Ga68-PSMA radiotracer uptake in gastric adenocarcinoma (Iacovitti CM et al., 2025) and gastrointestinal stromal tumor (GIST) (Vaz S, et al., 2018; Florou VA et al., 2024) among others. Here we present a case of GIST initially detected on PSMA PET/CT.

Methods and Results: A 77-year-old male presented with elevated PSA. Prostate MRI demonstrated marked prostatomegaly with a PI-RADS 5 lesion spanning the entire left posterior peripheral zone, obliterating the ipsilateral neurovascular bundle and extending to the rectum. The prostate biopsy confirmed prostatic adenocarcinoma. F18-DCF-Pyl (Pylarify) PSMA PET/CT showed a focal radiotracer avid lesion at the prostate gland left posterior peripheral zone mid gland extending into the apex, SUV 21.3, consistent with the biopsy-proven prostatic adenocarcinoma (Figure 1). Incidentally, the same PSMA PET/CT scan also revealed a focal radiotracer-avid exophytic extraluminal soft tissue mass abutting the stomach lesser curvature, SUV 21.8, measuring approximately 3.9 x 2.5 cm (Figure 2). Contrast-enhanced CT confirmed a 3.8 x 2.6 cm exophytic extraluminal soft tissue mass inseparable from the lesser curvature of the stomach, suspicious for a primary gastric tumor (Figure 3). Endoscopic ultrasound-guided biopsy of the gastric mass revealed spindle cell neoplasm, consistent with a low grade gastrointestinal stromal tumor (GIST).

Discussions: Nonprostatic diseases, both benign and malignant tumors may demonstrate increased PSMA expression (de Galiza Barbosa F et al., 2020). A clinical trial study utilized F18-DCFPyL PET/CT to evaluate patients with colon, gastric and pancreatic cancer. This study detected the primary tumor in 7 out of 10 patients with colon, gastric and pancreatic cancer (Vuijk et al., 2022). GIST have also been reported as incidental findings on PSMA PET/CT in patients with prostate cancer (Lee DJW et al., 2021; Laurens ST et al., 2018; Jaleel J et al., 2023; Iversen P et al., 2022; Sasikumar A et al., 2017). However, high physiological PSMA radiotracer

background uptake in the gastrointestinal tract may limit the ability of detecting the primary gastric tumor.

Conclusion: This case highlights the feasibility of detecting gastrointestinal cancers with F18-DCF-Pyl (Pylarify) PSMA PET/CT. Incidental gastric tracer uptake should not be dismissed, as it may represent neoplastic lesions such as GIST. The expression of PSMA on GIST suggests potential future theranostic applications.

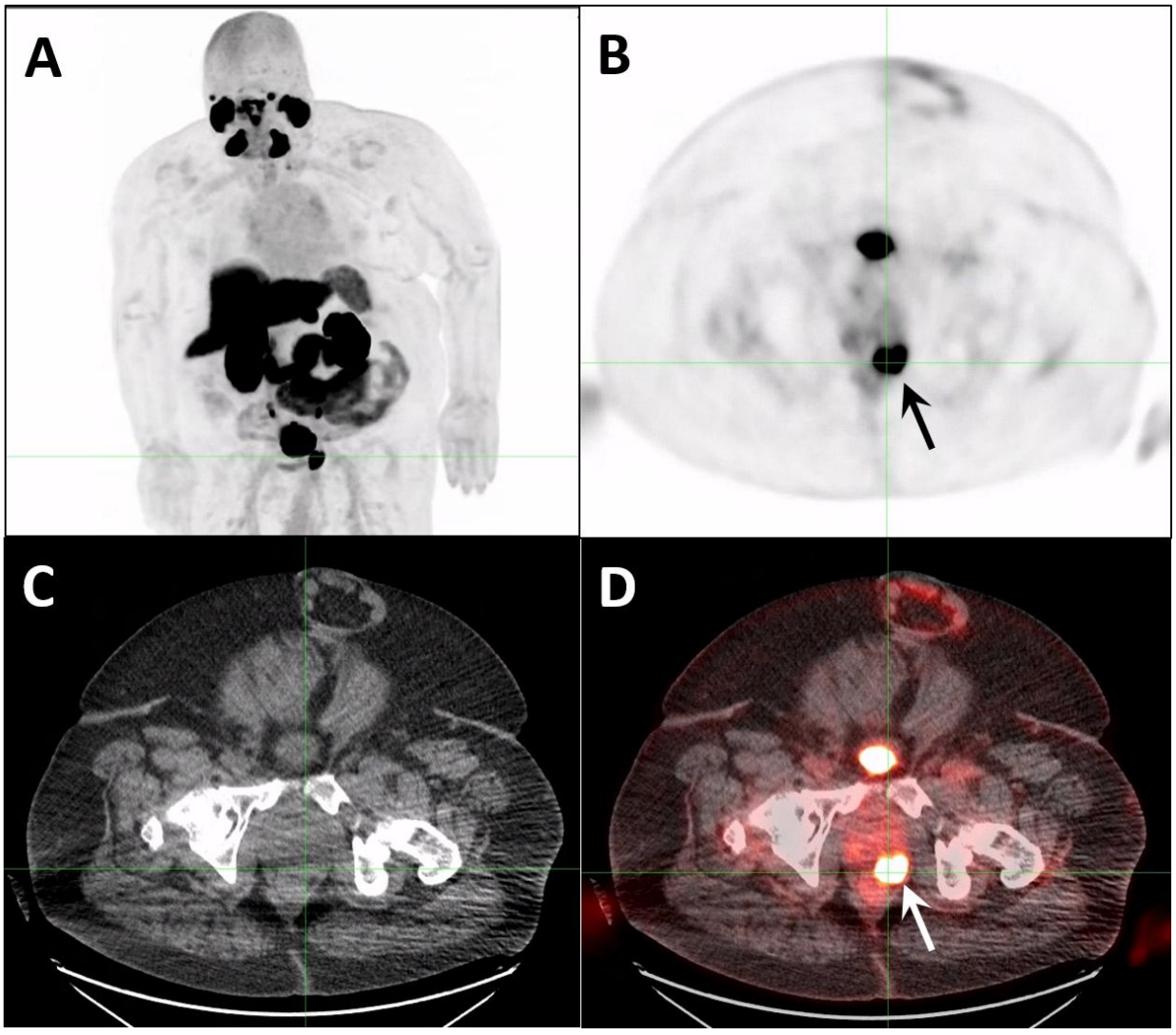

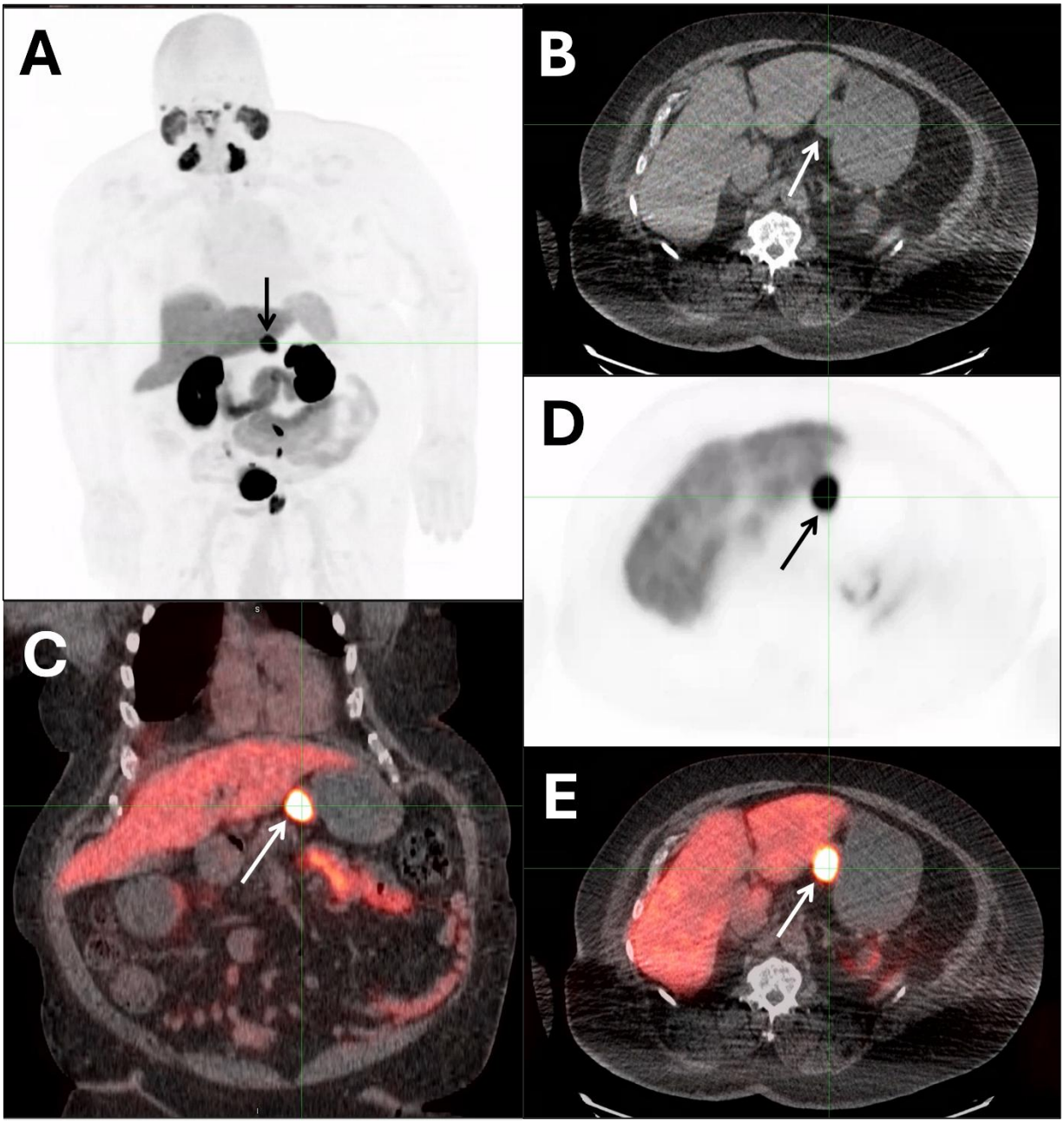
A
B
C
D
E

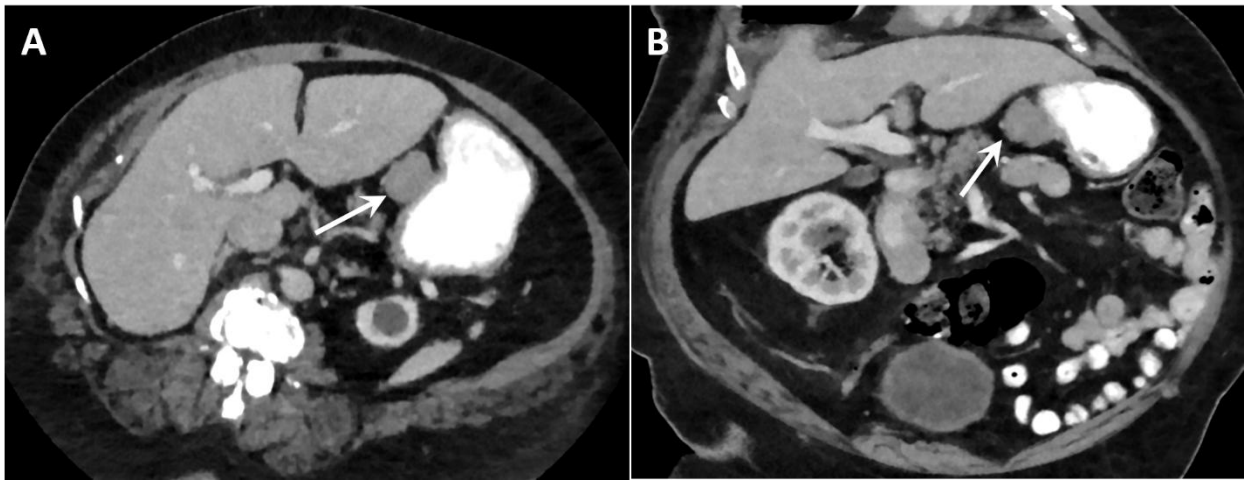

Reference

1. Haffner MC, Kronberger IE, Ross JS, Sheehan CE, Zitt M, Mühlmann G, Ofner D, Zelger B, Ensinger C, Yang XJ, Geley S, Margreiter R, Bander NH. Prostate-specific membrane antigen expression in the neovasculature of gastric and colorectal cancers. Hum Pathol. 2009 Dec;40(12):1754-61.
2. Iacovitti CM, Muoio B, Cuzzocrea M, Paone G, Treglia G. Gastric Adenocarcinoma Incidentally Detected by PET/CT with PSMA Ligands. Diagnostics (Basel). 2025 Jan 3;15(1):101.
3. Vaz S, Oliveira C, Castanheira JC, Silva ÂF, Costa DC. Gastric GIST Incidentally Detected on 68Ga-PSMA-PET/CT: Correlation Between Functional Imaging and Histology. Clin Nucl Med. 2018 Dec;43(12):e488-e491.
4. Florou VA, Reyes DK, Pienta KJ. Incidental discovery of gastrointestinal stromal tumor via PSMA-PET/CT imaging: Insights from a case report. Urol Case Rep. 2024 Dec 31;58:102926.
5. de Galiza Barbosa F, Queiroz MA, Nunes RF, Costa LB, Zaniboni EC, Marin JFG, Cerri GG, Buchpiguel CA. Nonprostatic diseases on PSMA PET imaging: a spectrum of benign and malignant findings. Cancer Imaging. 2020 Mar 14;20(1):23.
6. Vuijk FA, Kleiburg F, Noortman WA, Heijmen L, Feshtali Shahbazi S, van Velden FHP, Baart VM, Bhairosingh SS, Windhorst BD, Hawinkels LJAC, Dibbets-Schneider P, Bouwman N, Crobach SALP, Fariña-Sarasqueta A, Marinelli AWKS, Oprea-Lager DE, Swijnenburg RJ, Smit F, Vahrmeijer AL, de Geus-Oei LF, Hilling DE, Slingerland M. Prostate-Specific Membrane Antigen Targeted Pet/CT Imaging in Patients with Colon, Gastric and Pancreatic Cancer. Cancers (Basel). 2022 Dec 15;14(24):6209.
7. Lee DJW, Warner M, Shannon T, Moschilla J. Incidental finding of ileal gastrointestinal stromal tumour during prostate cancer staging with prostate-specific membrane antigen scan. J Med Imaging Radiat Oncol. 2021 Feb;65(1):89-91.

8. Laurens ST, Witjes F, Janssen M, Flucke U, Gottardt M. 68Ga-Prostate-Specific Membrane Antigen Uptake in Gastrointestinal Stromal Tumor. Clin Nucl Med. 2018 Jan;43(1):60-61.
9. Jaleel J, Subudhi TK, Sagar S, Yadav R, Tripathi M, Bal C. Incidentally Detected Gastrointestinal Stromal Tumor in a Patient with Carcinoma Prostate: ^{68}Ga-Prostate-Specific Membrane Antigen Versus ^{18}F-Fluorodeoxyglucose Positron Emission Tomography/Computed Tomography. Indian J Nucl Med. 2023 Jan-Mar;38(1):67-68.
10. Iversen P, Hansen AK, Hubeck-Graudal T, Medrud L, Bouchelouche K. PSMA-Positive Low Malignant Gastrointestinal Stromal Tumor in the Stomach on F-18-PSMA-1007 PET/CT. Diagnostics (Basel). 2022 Jan 18;12(2):227.
11. Sasikumar A, Joy A, Pillai M, S B, Sr S. 68Ga-PSMA Uptake in an Incidentally Detected Gastrointestinal Stromal Tumor in a Case of Suspected Carcinoma Prostate. Clin Nucl Med. 2017 Oct;42(10):e447-e448.

POSTER #1

Title: Pseudo-Degenerative Uptake: A Nuclear Medicine Pitfall.

Eduardo Sanchez-Perez, MD

Ana Y. Valdivia, MD

Montefiore Medical Center, Nuclear Medicine Division, Department of Radiology, Montefiore Medical Center, The University Hospital for Albert Einstein College of Medicine, Bronx, NY 10461

E-mails: esanchezpe@montefiore.org, avaldivi@montefiore.org

Background:

Enthesopathy, arthritis, and bursitis – often labeled as degenerative on imaging – are common, age-related musculoskeletal conditions that can significantly impair function (1-2). Nuclear Medicine studies, frequently performed in older oncologic patients, can sensitively detect inflammation in joints, ligaments, tendons, and bursae (2-3). However, these findings are often overlooked in practice due to their prevalence and limited relevance to the primary clinical question. This case series highlights potential pitfalls in such scenarios.

Method:

A retrospective analysis was performed on two patients whose radiotracer uptake initially suggested degenerative joint disease but was later confirmed to be malignant.

Results:

Case 1: A 76-year-old woman with recurrent T8 paraspinal and right T8 pericostal plasmacytomas, previously treated with surgery and radiation, underwent follow up 18F-FDG PET/CT (Figure 1A), showing treatment response, a same-level vertebral compression fracture and intense L2-L3 interspinous uptake suggestive of bursitis. Because the patient complained of persisting lower back pain, lumbar spine MRI (Figure 1B) revealed recurrent disease. A subsequent PET/CT (Figure 1C) showed worsening intense diffuse uptake in the L2 spinous process, consistent with a malignant marrow replacing lesion, later treated with radiation.

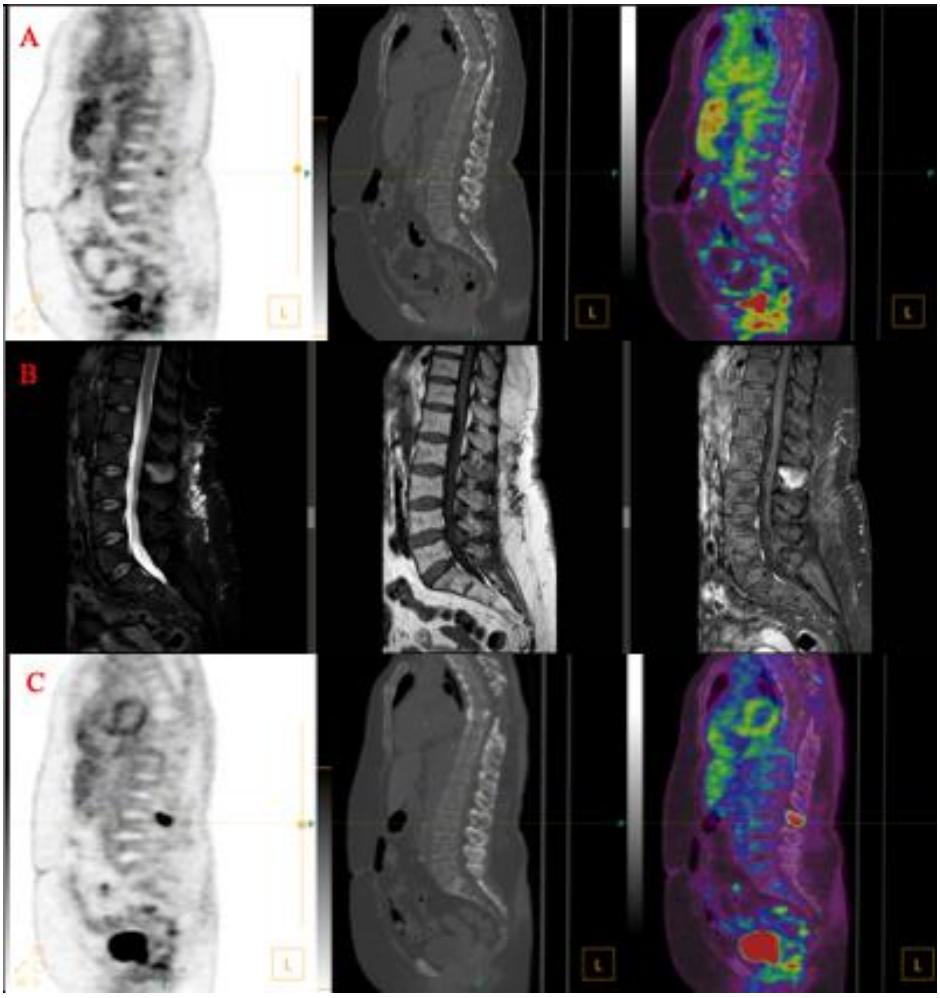

Figure 1: 18F-FDG PET/CTs and MRI of a 76-year-old woman with adequately treated recurrent plasmacytoma. (A) Sagittal PET, CT, and fused images show isolated FDG uptake at the L2-L3 interspinous region. (B) Sagittal T2, T1, and a post-contrast T1 MRI reveal an enhancing T2 hyperintense, T1 hypointense lesion in the L2 spinous process. (C) Sagittal images of a follow up PET/CT show worsening intense uptake throughout the L2 spinous process.

Case 2: 61-year-old man with recently diagnosed right breast adenocarcinoma with ipsilateral axillary nodal involvement who underwent staging bone scintigraphy (Figure 2A), which appeared negative aside from degenerative changes, including left > right shoulder uptake. Follow up 18F-FDG PET/CT (Figure 2B) showed intense focal uptake in a left acromial

hypodensity, consistent with metastasis. Biopsy confirmed breast adenocarcinoma.

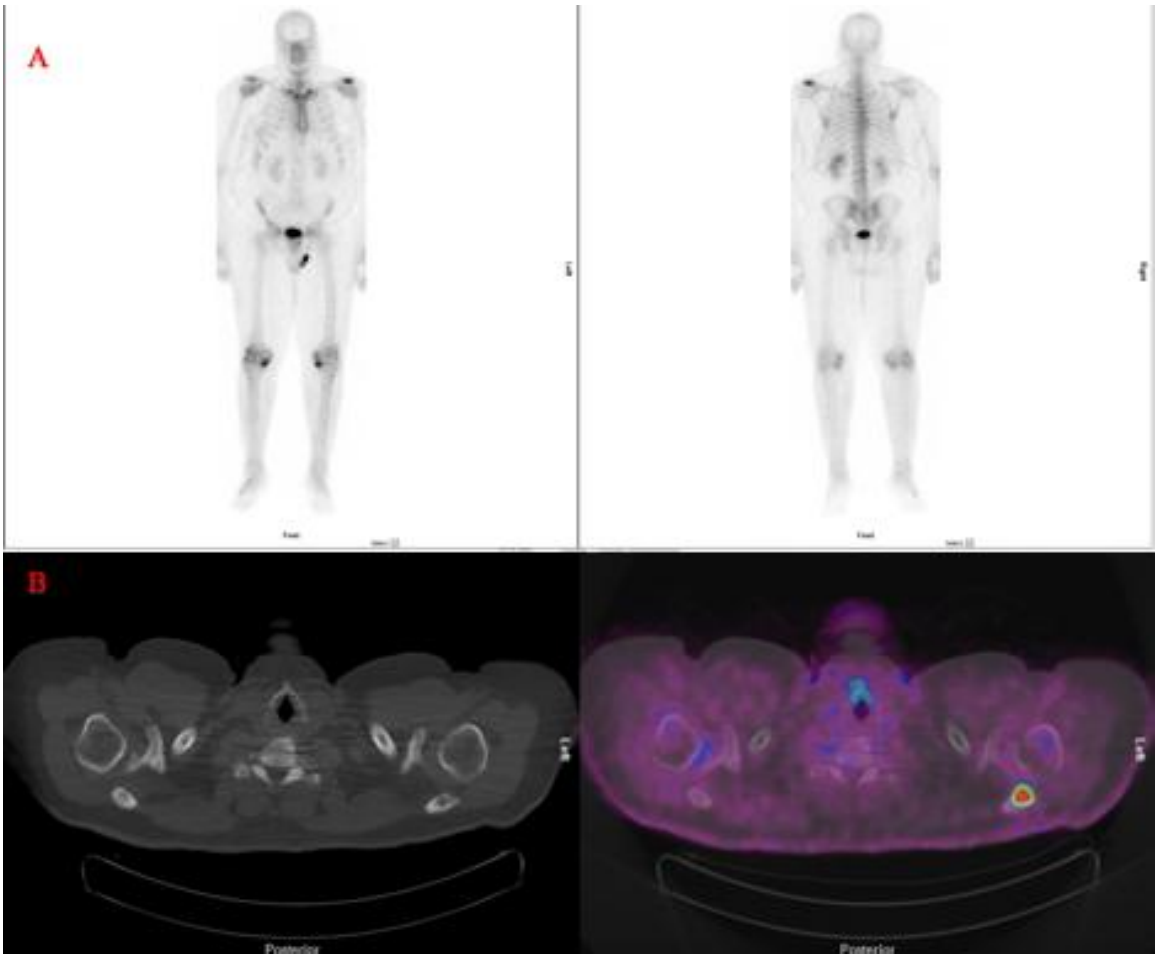

Figure 2: Bone scintigraphy and 18F-FDG PET/CT images of a 61-year-old man with newly diagnosed right breast adenocarcinoma. (A) Whole body planar images show symmetric degenerative joint disease uptake in multiple joints, including knees and sternoclavicular joints. The anterior view shows only subtle left > right shoulder uptake, while the posterior projection clearly demonstrates isolated increased uptake on the left shoulder. (B) Axial low-dose CT and fused PET/CT images at the level of the shoulders revealed a lucency in the left acromion with intense FDG uptake.

Discussion:

This case series highlights the pitfall of pseudo-degenerative uptake on nuclear medicine studies and underscores the need for a standardized approach to describing asymmetries and atypical sites of degenerative activity. As immunotherapies become more common, inflammatory uptake in joints, ligaments, and bursae is likely to increase, making such standardization potentially valuable in reducing misdiagnosis.

References:

1. Moshrif, A., Abdel Noor, R., Aly, H., Mortada, M., & Hafez, A. (2022). Aging and entheses: An ultrasonographic probing of degenerative enthesopathy in a cohort of 147 healthy subjects. *International journal of rheumatic diseases*, *25*(4), 481–488. https://doi.org/10.1111/1756-185X.14301
2. Fahmi, D.S., Makarm, W.K. & Zaghlol, R.S. (2022). Burden of enthesitis on the quality of life and work productivity in psoriatic arthritis patients. *Egypt Rheumatol Rehabil*49, 58. https://doi.org/10.1186/s43166-022-00157-7
3. Riccabona G. (1999). Nuclear medicine in diagnosis and therapy of bone and joint diseases. *Nuclear medicine review. Central & Eastern Europe*, *2*(1), 42–52.
4. Yamashita, H., Kubota, K., & Mimori, A. (2014). Clinical value of whole-body PET/CT in patients with active rheumatic diseases. *Arthritis research & therapy*, *16*(5), 423. https://doi.org/10.1186/s13075-014-0423-2

POSTER #2

Hyperkinetic Gallbladder on HIDA Scan: Clinical Outcomes in a Case Series of Patients with Elevated Gallbladder Ejection Fraction

Siddarth Ragupathi, MD, Alireza Mohseni, MD, Kwang J. Chun, MD, Renee M. Moadel, MD, and Syed Mahmood, MD

Division of Nuclear Medicine, Department of Radiology, Montefiore Medical Center, The University Hospital for Albert Einstein College of Medicine, Bronx, NY 10461

E-mails: sragupathi@montefiore.org, amohseni@montefiore.org, kchun@montefiore.org, rmoadel@montefiore.org, syemahmood@montefiore.org

Background:

Hyperkinetic biliary dyskinesia (HBD) is defined as a gallbladder ejection fraction (GBEF) ≥ 80% on hepatobiliary iminodiacetic acid (HIDA) scan. While cholecystectomy is standard treatment for biliary hypokinesia or chronic cholecystitis, literature supports surgical management in patients with hyperkinetic gallbladder function, even in the absence of gallstones. This case series evaluates the clinical course and outcomes of HBD patients managed conservatively with medical and dietary interventions.

Methods:

A series of 7 patients with HBD on HIDA scan were retrospectively evaluated with 2-years of follow-up at Montefiore Medical Center. Clinical charts were reviewed for the referring service, patients' symptoms at presentation, radiology/nuclear medicine interpretation of the HIDA and other correlative imaging studies (ultrasound or CT), subsequent patient management, and patient outcomes.

Results:

Of the seven patients, five were referred by medical gastroenterology, one from surgical gastroenterology, and one from infectious disease. GBEFs ranged from 81 to 94.5%. Five patients (GBEFs 84-94%) experienced symptom improvement with conservative management measures, for example, dietary modification, antacids, and H2 blockers. One patient with an initial GBEF of 92% improved with dietary adjustments but experienced recurrent right upper quadrant pain three years later, at which time the GBEF was 82%, and this patient was re-referred to gastroenterology. Only one patient

with cholelithiasis had initial improvement with conservative therapy but eventually had symptom recurrence and ultimately underwent cholecystectomy.

Conclusions:

This small case series supports a tailored approach in the management of hyperkinetic biliary dyskinesia, starting with conservative management for all patients. In addition, our findings suggest that an elevated GBEF on HIDA scan may not necessarily warrant surgical intervention. In the absence of cholelithiasis, conservative management was helpful in symptomatic improvement in our case series cohort. Future directions include an evaluation of a multiyear patient cohort from our medical center to further evaluate the clinical significance of elevated GBEF, standardize our diagnostic reporting of hyperkinetic gallbladder on HIDA scan, and establish evidence-based guidelines for optimal patient management in patients presenting with hyperkinetic biliary dyskinesia.

POSTER #3

Abstract

Title:

Interictal ^{18}F-FDG-PET Hypometabolism concordance with EEG, MRI and Clinical Outcomes in Patients with Epilepsy

Authors:
Affaf Gul, MD; Shazia Naseem, MD; Renee M. Moadel, MD; Syed Mahmood, MD
Division of Nuclear Medicine, Department of Radiology
Montefiore Medical Center, The University Hospital for Albert Einstein College of Medicine
Bronx, NY 10461
Emails: agul@montefiore.org; snaseem@montefiore.org; rmoadel@montefiore.org; syemahmood@montefiore.org

Background:

Epilepsy, affecting approximately 50 per 100,000 individuals annually, is a common neurological disorder characterized by recurrent, unprovoked seizures resulting from abnormal, synchronized neuronal activity. Regardless of the cause, accurate localization of the epileptogenic focus is essential for effective management, particularly in patients considered for surgical intervention. Although the clinical history and neurological examination remain fundamental to the diagnosis, additional modalities such as electroencephalography (EEG) and neuroimaging with magnetic resonance imaging (MRI) and ^{18}F-fluorodeoxyglucose positron emission tomography brain scans (PET), play an essential role in identifying the seizure focus and determining the most appropriate therapeutic approach. Approximately one-third of patients develop medically intractable epilepsy, emphasizing the need for multimodal imaging approaches to improve diagnostic accuracy and guide presurgical evaluation for local resection of the seizure-generating area. [2] PET provides metabolic insights into areas of neuronal dysfunction, often showing hypometabolism in the epileptogenic zone in the interictal period. [3,4] PET is especially valuable when MRI and EEG findings are non-localizing or discordant. [5,6] The absence of standardized clinical management guidelines for intractable epilepsy subtypes underscores the ongoing need for research aimed at optimizing diagnostic accuracy and therapeutic outcomes.

Objective:

This is a retrospective observational cohort study of patients who underwent FDG PET brain scans between November 1, 2016, and June 30, 2025. Among patients who underwent a PET scan, those with a history of epilepsy were identified, and their clinical charts were reviewed for demographics, radiology/nuclear medicine interpretation of PET brain scans and MRI brain studies, patients' symptoms at presentation, where the PET was ictal or interictal, subsequent patient management, and patient outcomes. We hypothesized that interictal PET scans would show a high degree of concordance with EEG findings in localizing the epileptogenic zone to the same lobe or the same hemisphere.

Methods:

Following IRB approval, a retrospective chart review was conducted to identify all patients with a PET brain scan between November 1, 2016, and June 30, 2025 at Montefiore Medical Center. Patients with epilepsy were identified, and their clinical charts were reviewed for PET

and MRI interpretation by radiologists/nuclear medicine physicians, interpretation of EEG studies by neurologists, further management approach (surgical vs conservative), and follow-up outcomes of up to 2 years.

Results:

Among 19,157 PET brain scans, 167 patients had epilepsy, including 30 with medically intractable epilepsy.

Table 1. Summary of PET, EEG, and MRI Concordance and Clinical Outcomes in Patients with Intractable Epilepsy (n = 30)

Category	Finding	No. of Patients (n)	Percentage (%)
PET–EEG Concordance	Concordant PET and EEG	19	63.3
	No hypometabolism on PET	5	16.7
	Discordant localization	1	3.3
	Inconclusive/Non-localizing PET	5	16.7
Multimodal Concordance (PET–EEG–MRI)	Concordant PET, EEG, and MRI	8	26.7
	Concordant PET and EEG, discordant MRI	15	50.0
	Concordant MRI and PET, discordant EEG	5	16.7
	Discordant PET, concordant MRI and EEG	2	6.7
Management and Outcomes	Considered for surgery (based on PET/EEG concordance)	10	33.3
	Underwent surgery (with seizure reduction)	3	10.0
	Medically managed	16	53.3
	Responsive Neurostimulation (RNS) implanted	4	13.3
	RNS patients being considered for surgery	2	6.7

Conclusions:

Interictal ^{18}F-FDG PET is a valuable adjunct in the presurgical evaluation of epilepsy, by reliably localizing the interictal seizure focus and helping select patients most likely to achieve an improved outcome after surgical intervention. PET scans demonstrated a high rate of concordance (63.3%) with EEG in localizing epileptogenic foci. In addition, PET contributed unique localization data in 50% of cases where MRI findings were discordant or non-localizing, highlighting its utility in presurgical evaluation. Patients selected for surgery based on PET/EEG concordance experienced improved seizure control, supporting the role of

PET in predicting favorable outcomes. Larger prospective studies and standardized outcome metrics are warranted to validate PET-based criteria for surgical planning and long-term prognostication.

References:

1. Beghi E. The epidemiology of epilepsy. Neuroepidemiology. 2020;54(2):185-191. doi:10.1159/000503831
2. Kwan P, Arzimanoglou A, Berg AT, et al. Definition of drug-resistant epilepsy: Consensus proposal by the ad hoc Task Force of the ILAE Commission on Therapeutic Strategies. Epilepsia. 2010;51(6):1069-1077. doi:10.1111/j.1528-1167.2009.02397.x
3. Knowlton RC. The role of FDG-PET, ictal SPECT, and MEG in the epilepsy surgery evaluation. Epilepsy Behav. 2006;8(1):91-101. doi:10.1016/j.yebeh.2005.10.015
4. Chugani HT. Role of positron emission tomography in epilepsy. Curr Opin Neurol. 1998;11(2):145-152. doi:10.1097/00019052-199804000-00008
5. Cascino GD. Surgical treatment for epilepsy. Curr Opin Neurol. 2011;24(2):173-177. doi:10.1097/WCO.0b013e32834445d6
6. Bell ML, Rao S, So EL. Epilepsy surgery outcomes in temporal lobe epilepsy with a normal MRI. Epilepsia. 2009;50(9):2053–2060. doi:10.1111/j.1528-1167.2009.02066.x

POSTER #4

SUV Max and Tumor Staging in Screening-Detected Lung Cancers: Findings from a Community Program

Authors: Kevin Hricko BA MS MPH[1], Louis Mazzarelli MD[2], Karen Geary[3], Alexander Mazzarelli[4], Richard G. Barr MD[5]

Institutions: [1]University of Connecticut School of Medicine; [2]Department of Radiology, Lawrence and Memorial and Westerly Hospitals, Yale New Haven Health; [3]Lawrence and Memorial and Westerly Hospitals, Yale New Haven Health; [4]The Williams School; [5]Northeast Ohio Medical University and Southwoods Imaging

Email addresses: kevin.j.hricko@gmail.com, mazzarellilouis@gmail.com, Karen.Geary@lmhosp.org, amazzarelli@williamsschool.org, rgbarr525@gmail.com

Background

Lung cancer screening programs are critical for early detection and improved survival. PET imaging and maximal standard uptake values (SUV Max) provide insights into tumor metabolic activity. While extensively studied in symptomatic populations, SUV Max trends in screening-detected lung cancers remain underexplored. This analysis evaluates relationships between SUV Max, tumor staging, and survival outcomes in screening-detected lung cancers.

Methods

Retrospective analysis of 108 screening-detected lung cancers (104 patients, 5 synchronous cancers) from a community-based program (2017-2023). Patients underwent annual low-dose CT scans. Tumors were stratified by SUV Max thresholds (<4, 4-10, ≥10) and staging. Logistic regression and chi-square testing assessed prognostic significance of SUV Max and tumor size for mortality prediction, particularly in Stage 1 cancers.

Results

Among 108 tumors, 27.78% (30/108) exhibited SUV Max < 4, with 93.3% (28/30) classified as Stage 1 or 2. Of 30 patients with SUV Max < 4, 86.7% (26/30) were alive at median follow-up of 30 months (range: 6-88 months). Median time to death among deceased patients was 21 months. Tumors with SUV Max ≥ 10 demonstrated comparable survival to low-SUV tumors when detected at Stage 1 or 2 (87.76% vs. 86.67% alive). Logistic regression revealed SUV Max was not an independent mortality predictor after adjusting for staging ($p > 0.05$), while staging remained the strongest survival predictor ($p = 0.009$). Chi-square analysis ($p=1.0$) and odds ratios (OR=0.68, 95% CI: 0.06-8.25) confirmed no significant survival difference among Stage 1 tumors by SUV Max. Within Stage 1 cancers, neither tumor size (p

= 0.588) nor SUV Max (p = 0.369) independently predicted mortality. Stage 1 tumor sizes ranged from 0.4 to 3.8 cm (mean: 1.73 cm, median: 1.5 cm). Smaller Stage 1 tumors (≤2 cm) more commonly exhibited SUV Max < 10; lower SUV Max in smaller tumors may partially reflect volume averaging effects inherent to PET spatial resolution. Late-stage cancers exhibited poor survival regardless of SUV Max, underscoring limited prognostic utility of metabolic activity in advanced disease (Figure 1). Figure 2 illustrates a representative case.

Conclusion

Low SUV Max values (<4) were predominantly associated with early-stage disease (93.3%) and favorable survival. However, Stage 1-2 tumors with SUV Max ≥ 10 exhibited comparable survival to low-SUV tumors when treated early, emphasizing the importance of early detection. Statistical analysis confirmed staging, rather than SUV Max or tumor size, as the dominant survival predictor for early-stage cancers. High SUV Max likely reflects biologic aggressiveness, but timely treatment mitigates its impact. Future research should investigate biological drivers of high SUV Max in early-stage cancers and validate findings in multi-center cohorts.

FIGURES

Figure 1. Correlation of SUV Maximal Uptake with Lung Cancer Stage and Patient Mortality

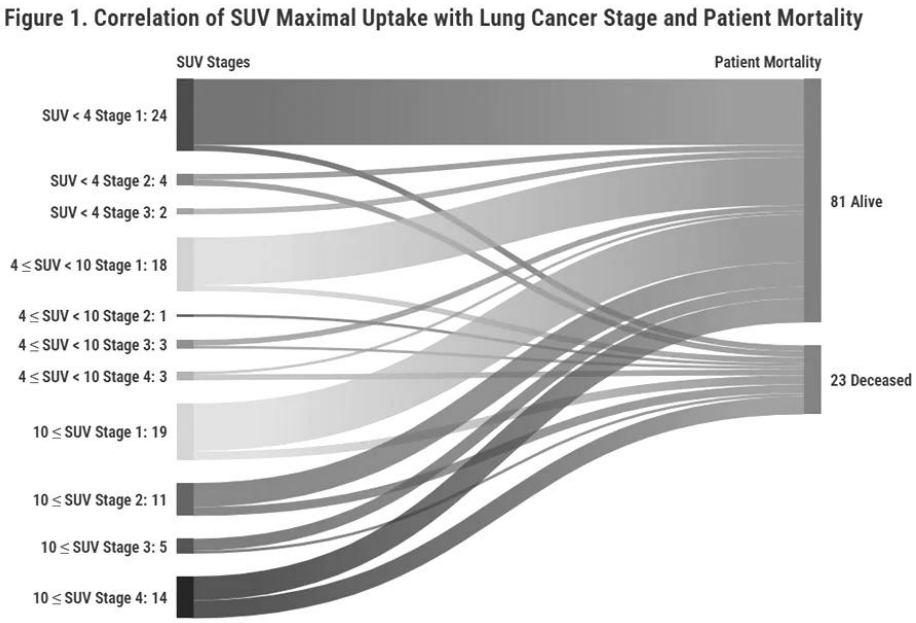

Sankey diagram illustrating the relationship between SUV Max categories (<4, 4-10, ≥10), tumor staging (Stage 1-4), and patient outcomes (alive vs. deceased) in 108 screening-detected lung cancers. The diagram demonstrates that low SUV Max values (<4) predominantly correlate with early-stage disease (Stage 1-2) and favorable survival outcomes. Notably, tumors with high SUV Max (≥10) detected at early stages showed comparable survival to low SUV tumors when treated promptly, emphasizing the critical role of early detection and intervention over metabolic activity in determining outcomes.

Figure 2. Screen Detected Stage 1A3 Lung Cancer with High SUV Max

61-year-old male with screen-detected Stage 1A3 adenocarcinoma demonstrating markedly elevated SUV Max of 40.16 despite early-stage disease. The patient underwent successful surgical resection without recurrence, illustrating that high metabolic activity in early-stage cancers does not preclude excellent outcomes when detected through screening and treated appropriately. This case exemplifies the study's key finding that staging, rather than SUV Max, is the dominant predictor of survival in screening-detected lung cancers.

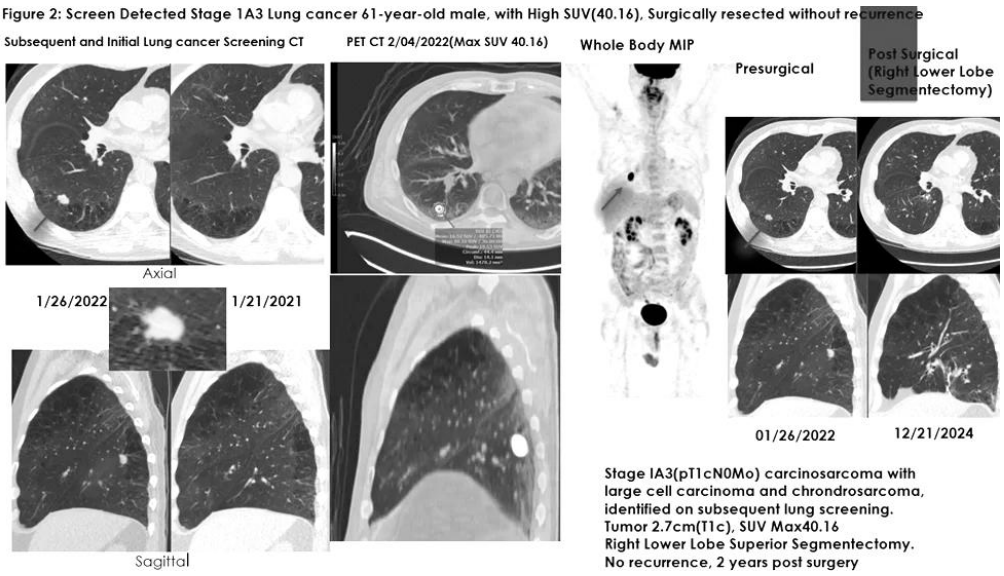

POSTER #5

Diagnostic Value of Routine Delayed Pelvic Imaging in ^{68}Ga-PSMA PET/CT Early Biochemical Recurrence of Prostate Cancer

Karen Jia[1], Jonathan Kuten[1], Josef Fox[1], Heiko Schoder[1],[1]
Ali Aria Razmaria[1]

[1]Molecular Imaging and Therapy Service, Department of Radiology, Memorial Sloan Kettering Cancer Center, New York, New York.

Background:
Detecting biochemical recurrence (BCR) of prostate cancer remains challenging, as small-volume disease may fall below the sensitivity of standard imaging. While ^{68}Ga-PSMA PET/CT offers excellent detection even at low PSA levels, current guidelines recommend only a single acquisition at 60 minutes post-injection. We evaluated whether routine delayed pelvic imaging at 90 minutes improves diagnostic performance in early BCR.

Methods:
We retrospectively analyzed 201 patients with prostate cancer undergoing dual-phase ^{68}Ga-PSMA PET/CT for early BCR (median PSA 0.52 ng/mL). Whole-body imaging was acquired at approximately 60 minutes and delayed pelvic imaging at approximately 90 minutes post-injection. Two nuclear medicine physicians independently assessed whether delayed imaging improved diagnostic certainty or revealed additional PSMA-avid lesions.

Results:
Delayed pelvic imaging improved diagnostic certainty in 34% (68/201) of scans and revealed additional PSMA-avid lesions in 11% (23/201). Most new findings were pelvic lymph nodes (n = 13), followed by seminal vesicle (n = 5) and prostate bed recurrences (n = 5). Improvements were primarily due to (1) increased tracer uptake confirming subtle lesions, (2) reduced bladder or ureteral interference, and (3) differentiation of physiologic from pathologic uptake.

Conclusion:
Routine delayed pelvic imaging at 90 minutes enhances lesion detection and diagnostic confidence in patients with BCR, particularly at PSA values < 1 ng/mL. Incorporating this additional acquisition into standard PSMA PET/CT protocols can improve staging accuracy and clinical decision-making at the early window of minimal disease burden. Future efforts should assess streamlining workflows to facilitate adoption of dual-phase imaging at various practice settings.

POSTER #6

Title: Brain SPECT/CT With Acetazolamide (Diamox) in Management of Patients With Moyamoya Disease.

Zahra Karimi, MD, Affaf Gul, MD, Siddarth Ragupathi, MD, Kwang J Chun, MD, Ana Valdivia, MD.

Department of Radiology, Division of Nuclear Medicine, Montefiore Medical Center/ The University Hospital for Albert Einstein College of Medicine.

Background:

Brain SPECT/CT with acetazolamide (Diamox) challenge is a non-invasive imaging technique used to assess cerebrovascular reserve (CVR) in patients with moyamoya disease. Moyamoya is a progressive steno-occlusive vasculopathy of the cerebral vessels, most commonly involving the internal carotid arteries and their proximal branches, leading to compromised cerebral perfusion and risk of ischemic events (1). SPECT imaging at baseline and post-acetazolamide evaluates regional cerebral blood flow and the brain's ability to increase perfusion under vasodilatory stress. A diminished response after Diamox indicates impaired CVR, identifying brain regions at risk and aiding decisions about revascularization surgery (2).

Methods:

We present five clinical cases demonstrating the use of brain SPECT/CT with Diamox in the diagnosis, risk stratification, and management planning for patients with moyamoya disease.

Results:

Case 1: A 36-year-old woman presented with a left MCA syndrome and was found to have a left basal ganglia infarction on brain MRI and bilateral M1 occlusions on MRA head. Subsequent Digital Subtraction Angiography demonstrated moyamoya pattern with ACA/PCA collaterals. Patient was referred to nuclear medicine department for Brain SPECT/CT with Diamox for evaluation of ischemia prior to surgical intervention. The scan showed reduced uptake in the left corona radiata and basal ganglia, worsening with Diamox, indicating ischemia. The patient underwent successful left STA-MCA bypass surgery.

Case 2: A 20-year-old female with sickle cell disease and moyamoya disease presented with possible disease progression in the right MCA on follow up MRA. Brain SPECT/CT with Diamox demonstrated preserved cerebral perfusion and appropriate vascular reactivity,

suggesting sufficient CVR and no immediate need for surgical intervention. Ongoing medical management was maintained.

Case 3: A 43-year-old woman presented with right-sided weakness and was found to have a left MCA infarct with M1 occlusion on brain MRA. CT perfusion showed adequate collateral circulation. Brain SPECT/CT with Diamox revealed decreased perfusion in the left basal ganglia and cortical regions post-Diamox, although overall CVR appeared preserved with adequate symmetric cerebral blood volume increases. The patient didn't require any surgical intervention.

Case 4: A 12-year-old female with developmental delays and episodes of right-sided weakness was diagnosed with moyamoya on MRI. Brain SPECT/CT with Diamox showed decreased perfusion in the left sensorimotor cortex, parietal, and temporal lobes with appropriate vascular reactivity on post Diamox scan, suggesting sufficient CVR. The patient has not had any follow-up visits after the scan.

Case 5: A 48-year-old woman with chronic headaches and pre-syncopal episodes had angiographic evidence of left ICA stenosis. Workup for vasculitis was negative. Brain SPECT/CT with Diamox showed preserved perfusion and normal CVR. The patient continued medical management for ICA stenosis.

Conclusion:

Brain SPECT/CT with acetazolamide is a clinically effective tool for assessing cerebrovascular reserve in moyamoya disease. It helps identify patients with impaired vasodilatory capacity who are at increased risk for ischemic events and may benefit from surgical revascularization. While 15O-water PET remains the preferred modality for quantifying cerebral perfusion and CVR, its practical limitations make SPECT/CT a widely accessible and reliable alternative for guiding management and monitoring outcomes in this patient population (3,4).

References

1) Ihara M, Yamamoto Y, Hattori Y, Liu W, Kobayashi H, Ishiyama H, Yoshimoto T, Miyawaki S, Clausen T, Bang OY, Steinberg GK, Tournier-Lasserve E, Koizumi A. Moyamoya disease: diagnosis and interventions. Lancet Neurol. 2022 Aug;21(8):747-758.
2) Latchaw RE, Yonas H, Hunter GJ, Yuh WT, Ueda T, Sorensen AG, Sunshine JL, Biller J, Wechsler L, Higashida R, Hademenos G; Council on Cardiovascular Radiology of the American Heart Association. Guidelines and recommendations for perfusion imaging in cerebral ischemia: A scientific statement for healthcare professionals by the

writing group on perfusion imaging, from the Council on Cardiovascular Radiology of the American Heart Association. Stroke. 2003 Apr;34(4):1084-104.
3) Roder C, Bürkle E, Ebner FH, Tatagiba M, Ernemann U, Buck A, Meyer PT, Khan N. Estimation of Severity of Moyamoya Disease with [15O]Water-Positron Emission Tomography Compared with Magnetic Resonance Imaging and Angiography. World Neurosurg. 2018 Sep;117:e75-e81.
4) Acker G, Lange C, Schatka I, et al. Brain perfusion imaging under acetazolamide challenge for detection of impaired cerebrovascular reserve capacity: positive findings with (15)O-water PET in patients with negative (99m)Tc-HMPAO SPECT findings. J Nucl Med. 2018;59(2):294-298.

POSTER #7

Preventing Errors in Administered Radiopharmaceutical Doses in Nuclear Medicine

Ghazaleh Mehdipour, MD[1], Kwang J. Chun, MD[2]

1. Department of Radiology, Saint Vincent Medical Center, Hartford HealthCare, Quinnipiac University, CT

2. Division of Nuclear Medicine, Department of Radiology, Montefiore Medical Center, NY

Abstract:

Background: Misadministration of radiopharmaceuticals involves errors in the use of these agents for diagnostic or therapeutic purposes. Such errors include using the wrong radiopharmaceutical, giving it to the wrong patient, administering an incorrect dose, using the wrong route, or giving a dose to an unintended patient. A dosage differing by >50% from the prescribed amount for diagnostic procedures, or by >10% for therapeutic procedures, is considered a misadministration. The International Atomic Energy Agency (IAEA) specifies a threshold of 25% for therapeutic doses. These errors can result in unnecessary radiation exposure, incorrect or delayed diagnosis, increased healthcare costs, and irreversible harm to patients.

Methods: We conducted a literature review using PubMed to identify evidence on the causes of radiopharmaceutical misadministration and effective quality improvement (QI) strategies in nuclear medicine. We analyzed the potential causes of misadministration and implemented QI strategies to enhance safety protocols across the nuclear medicine division.

Results: The contributing factors to misadministration included failure to verify patient identifiers, communication lapses particularly during transitions between admitting, preparation, and scanning when patient identity and scan purpose were not consistently confirmed, lack of barcoding systems, and high clinic workload. Additional sources of error stemmed from the Language barriers within a diverse patient population. Differences in workflows between outpatient and inpatient settings led to inconsistent verification and safety practices. Contributing factors included variations in equipment, uneven staff training, and limited resources, such as the lack of a wristband printer.

We developed a QI plan and designed adaptable protocols to accommodate the unique challenges of each site. The intervention focused on standardizing patient identification protocols, improving staff training, and integrating verification steps, such as wristband use, to prevent radiopharmaceutical misadministration. A key component was strengthening the safety culture by encouraging staff to proactively identify and address potential errors and patient concerns. For therapeutic procedures, a checklist was designed to verify the correct radiopharmaceutical, dosage, and patient identifiers. Two independent team members were required to verify the dose

and patient identity. Monthly safety meetings were proposed to engage staff in discussions about safety, protocol adherence, and near-miss events.

Conclusions: Misadministration of radiopharmaceuticals is a preventable issue. As nuclear medicine studies and therapies continue to expand in volume and complexity, strict adherence to safety guidelines and proactive quality assurance remain essential.

POSTER #8

Unexpected PSMA Uptake within the Spleen: A Case Report and Review of the Literature

Stephen J. Sozio, DO, MBS[1], William Y. Raynor, MD[1], Levi Sokol, MD[1], Dhruv Patel, MD[1], Jeffrey S. Kempf, MD, FACR[1]

1. Rutgers Health, Rutgers Robert Wood Johnson Medical School, Department of Radiology, New Brunswick, NJ 08901

Background: PSMA is a transmembrane glycoprotein expressed on the surface of both prostate epithelial and prostate cancer cells, physiologically serving an array of functions related to cell metabolism, proliferation, and survival [1]. While PSMA PET/CT has become the cornerstone for staging and restaging of prostate cancer, it is important to recognize that PSMA uptake can also be seen in a variety of extra-prostatic infectious, inflammatory, and neoplastic processes, in addition to prostate cancer [1,2]. Splenic lesions with PSMA uptake can represent a diagnostic challenge, as several splenic pathologies unrelated to prostate metastasis can exhibit PSMA uptake. Thus, it is important for the radiologist to be aware of the differential diagnosis of PSMA uptake within the spleen.

Methods: A retrospective chart review was performed of a patient who underwent PSMA PET/CT which revealed a PSMA-avid splenic lesion. Relevant clinical history and imaging findings were reviewed. In addition, current literature regarding PSMA uptake in splenic lesions was also reviewed.

Results: A 73-year-old male underwent PSMA PET/CT for restaging of recurrent prostate adenocarcinoma. The patient initially completed pelvic radiation therapy six years ago, and now presented with a progressively rising PSA up to 3.6 ng/mL at the time of imaging. In addition to intraprostatic tumoral uptake with maximum SUV up to 16.8, a 2 cm PSMA-avid splenic lesion was discovered with maximum SUV up to 9.1. No additional focus of abnormal PSMA uptake was visualized outside the prostate. Subsequent contrast enhanced MRI abdomen revealed T2 hyperintense lesion with progressively increasing nodular post-contrast enhancement compatible with a splenic hemangioma corresponding to previously noted PSMA-avid splenic mass.

Discussion: A review of the literature revealed a reported incidence of splenic metastasis in the setting of prostate cancer of approximately 1-5%, most commonly in the setting of disseminated metastatic disease. PSMA uptake within spleen has also been reported in varied etiologies including splenic hemangioma, granulomatous disease, and splenosis, as well as prostate cancer metastasis [3,4,5,6,7]. Since the incidence of splenic hemangiomas has been reported up to 14%, PSMA uptake within these lesions may be increasingly detected on PSMA PET/CT [3].

Conclusions: Solitary focal splenic uptake on PSMA PET/CT can be due to a non-malignant process, such as a hemangioma. Correlation with other imaging findings, clinical history, prior imaging, and potentially histopathology, is essential when focal PSMA uptake is visualized within the spleen.

References:

1. Athiraman H, Miller K, Guido J, et al. “Unusual Prostate-Specific Membrane Antigen (PSMA) Splenic Uptake in a Patient with Prostate Cancer.” *Cureus*, 2024; 16(10):e70751.
2. Galiza Barbosa F, Queiroz MA, Nunes RF, et al. “Nonprostatic diseases on PSMA PET imaging: a spectrum of benign and malignant findings.” *Cancer Imaging*, 2020; 20(23).
3. Chausse G, Laufer J, Gad A, et al. “Splenic Hemangioma as a Potential Pitfall on PSMA-Targeted 18F-DCFPyL PET/CT.” *Clinical Nuclear Medicine*, 2019; 44(3):255-56.
4. Alsaleh MH, Alkhars AS, Albensaad M, et al. “Incidental detection of synchronous benign hepatic and splenic hemangiomas on 18F-PSMA PET/CT.” *Clinical Nuclear Medicine*, 2024; 49:e298–300.
5. Nearchou M, Georgiou E, Vrachimis A, et al. “Case Report: Post-traumatic splenosis and potential pitfall for PSMA-PET.” *Frontiers in Nuclear Medicine*, 2023; 3(1).
6. Budczies J, von Winterfeld M, Klauschen F, Bockmayr M, Lennerz JK, Denkert C, Wolf T, Warth A, Dietel M, Anagnostopoulos I, Weichert W. “The landscape of metastatic progression patterns across major human cancers.” *Oncotarget*, 2014: *6*(1), p.570
7. Comperat E, Azzouzi AR, Chartier-Kastler E, Menegaux F, Capron F, Richard F, Charlotte F. “Late Recurrence of a Prostatic Adenocarcinoma as a Solitary Splenic Metastasis.” *Urology International*, 2007; 78(1): 86-88.

POSTER #9

Concordance Between Visual Interpretation and Centiloid Quantification of Amyloid PET/CT in a Retrospective Quality Improvement Study

William Y. Raynor, MD[1], Andrew Soliman, MD[1], Levi Sokol, MD[1], Jeffrey S. Kempf, MD, FACR[1]

Department of Radiology, Rutgers Health,
Robert Wood Johnson Medical School New Brunswick, NJ, USA.

Background: Amyloid PET/CT has become increasingly integrated into clinical practice for guiding anti-amyloid therapy in patients with mild cognitive impairment. Historically, visual interpretation using a binary read of visually positive or visually negative has been used to determine amyloid positivity. More recently, quantitative analysis using the standardized Centiloid (CL) scale has been adopted clinically as a complementary tool to visual reads, allowing for more objective and reproducible assessments as well as for assessment of response to anti-amyloid therapy. This retrospective quality improvement study aimed to determine the degree of concordance between visual interpretation alone and a CL-based analysis of amyloid PET/CT studies, in addition to identifying sources of discordance.

Methods: A retrospective review was performed of amyloid PET/CT studies (using ^{18}F-florbetapir and ^{18}F-florbetaben) obtained at our institution between June 3, 2025, and September 3, 2025. Visual reads were performed at the time of scanning without access to quantitative data. CL values were retrospectively calculated for each scan using MIMneuro (MIM Software Inc., Cleveland, OH), and a threshold of 24.4 CL was applied to determine positivity. Additional subgroup analyses were conducted for cases with CL values falling inside and outside an intermediate range defined as 10-40 CL. Discordant cases were reviewed by two independent readers to determine the causes of discordance.

Results: Fifty scans were included in this study (38 using ^{18}F-florbetapir, 12 using ^{18}F-florbetaben). Of these, 29 were visually interpreted as positive and 21 as negative. Using the 24.4 CL threshold, 46 of 50 scans (92%) demonstrated concordance between the visual read and quantitative analysis, while 4 of 50 (8%) were discordant. Four scans total had CL values within the intermediate zone; among these, 2 (50%) were concordant and 2 (50%) discordant. Excluding the intermediate zone, 44 of 46 scans (95.7%) were concordant and 2 of 46 (4.3%) discordant. Review of discordant cases identified one error in visual analysis: a case with 68.63 CL was visually interpreted as negative due to significant cerebral atrophy, mimicking a white matter pattern on PET images. Three errors in quantification were also identified. Specifically, a case with 48.66 CL was visually negative, but the quantified gray matter activity in the cerebrum was falsely elevated due to a large retrocerebellar cyst affecting the reference region. In addition, a case with 23.67 CL (intermediate zone) was visually positive, with a chronic left frontal infarct causing underestimation of the quantified amyloid involvement. Lastly, a case with 22.99 CL (intermediate zone) was visually positive with likely early amyloid deposition, although below the quantitative threshold for positivity.

Conclusions: There was a high level of concordance (92%) between visual interpretation and CL quantification of amyloid PET/CT studies performed at our institution, supporting the validity of

visual analysis. Atrophy was the significant contributor to visual misinterpretation, while quantification errors were related to unexpected pathology (e.g., retrocerebellar cyst, chronic infarct) affecting reference or target regions. These findings highlight the complementary value of visual and quantitative approaches and underscore the need for continued refinement of quantification methods to address anatomic variants and pathology.

POSTER #10

^{18}F-Florbetapir Amyloid PET Quantification Remains Stable with Shorter Acquisition Times

Alfredo Lucas[1], Rebecca Ward[1,2], Safiya I. Lahlaf[1,2], Jacob Dubroff[1,2], Austin Pantel[1,2], Ilya Nasrallah[1,2], and Philipose G. Mulugeta[1,2]

University of Pennsylvania, Perelman School of Medicine[1]; Department of Radiology[2]

Background: ^{18}F-florbetapir amyloid PET directly quantifies brain beta-amyloid, identifying the hallmark early pathologic change of Alzheimer's disease. Standard ^{18}F-florbetapir imaging is performed with a 10-minute PET acquisition started 30-50 minutes after administration of a 10mCi dose. This study explored whether reducing the PET acquisition duration from 10 minutes significantly affected the amyloid PET quantitative burden of amyloid plaque measured by the standardized Centiloid score. Shorter PET acquisition times could help increase patient comfort and clinical throughput. Validation of short image times could also inform dose reduction strategies at 10-minute acquisition times, optimizing ALARA and radiopharmaceutical costs.

Methods: This study was IRB approved. We prospectively gathered and anonymized dynamic ^{18}F-florbetapir amyloid PET images from 21 patients. Each dynamic acquisition consisted of 10 one-minute frames acquired 30-50 minutes after injection of 10mCi of ^{18}F-florbetapir acquired on a Biograph Vision PET/CT scanner (Siemens Healthineers, Erlangen, Germany). From the dynamic images, we reconstructed 1-minute, 2-minute, 5-minute, and 10-minute images by averaging the number of blocks corresponding to the desired duration of acquisition (e.g., the 5-minute reconstruction consisted of the average of the first 5 one-minute acquisitions). For all reconstructions, we computed the Centiloid score (CL) using the FDA-approved MIM Software version 7.3.4 (MIM Software, Cleveland, Ohio). We used the clinical read as the gold standard, and a CL threshold of 25 for classifying cases as quantitatively positive or negative for moderate to frequent amyloid neuritic plaques.

Results: The estimated signal-to-noise ratio (SNR) increased proportionally to the acquisition duration, with the 1-minute reconstruction having the lowest SNR (0.87±0.20) and the 10-minute reconstruction the highest (2.04±0.43) (Figure 1A,B). Despite this trend, there was no significant difference between the CL values measured at 1, 2, 5, and 10-minute reconstructions (ANOVA $F=0.04$, $p=0.986$). The mean CL difference relative to the 10-minute reconstruction, for 1, 2, and 5-minute reconstructions was -0.2±15.6, -4.9±12.7, and -3.7±6.5 (Figure 1C). Using a CL threshold of 25, the sensitivity, specificity, and accuracy for 1-, 2-, 5-, and 10-minute reconstructions were 0.91/0.80/0.86 (2 false negatives, 1 false positive), 1.00/0.82/0.90 (2 false negatives), 1.00/0.82/0.95 (1 false negative), and 1.00/0.90/0.95 (1 false negative), respectively (Figure 1D).

Conclusion: Reducing ^{18}F-florbetapir PET acquisition duration from the standard 10 minutes to as short as 1–2 minutes does not significantly alter quantitative amyloid burden estimates as measured by Centiloid score. The FDA-cleared MIM Software CL quantification pipeline showed high consistency across all acquisition durations, with comparable sensitivity and specificity for amyloid positivity classification. While shorter scans exhibited lower signal-to-noise ratios, these differences did not meaningfully impact centiloid quantification. These results suggest that ^{18}F-florbetapir amyloid PET acquisition times could be shortened on high resolution PET/CT scanners without compromising quantitative accuracy, thus enabling improved patient throughput, reduced scanner time, and lower operational costs in clinical and research settings.

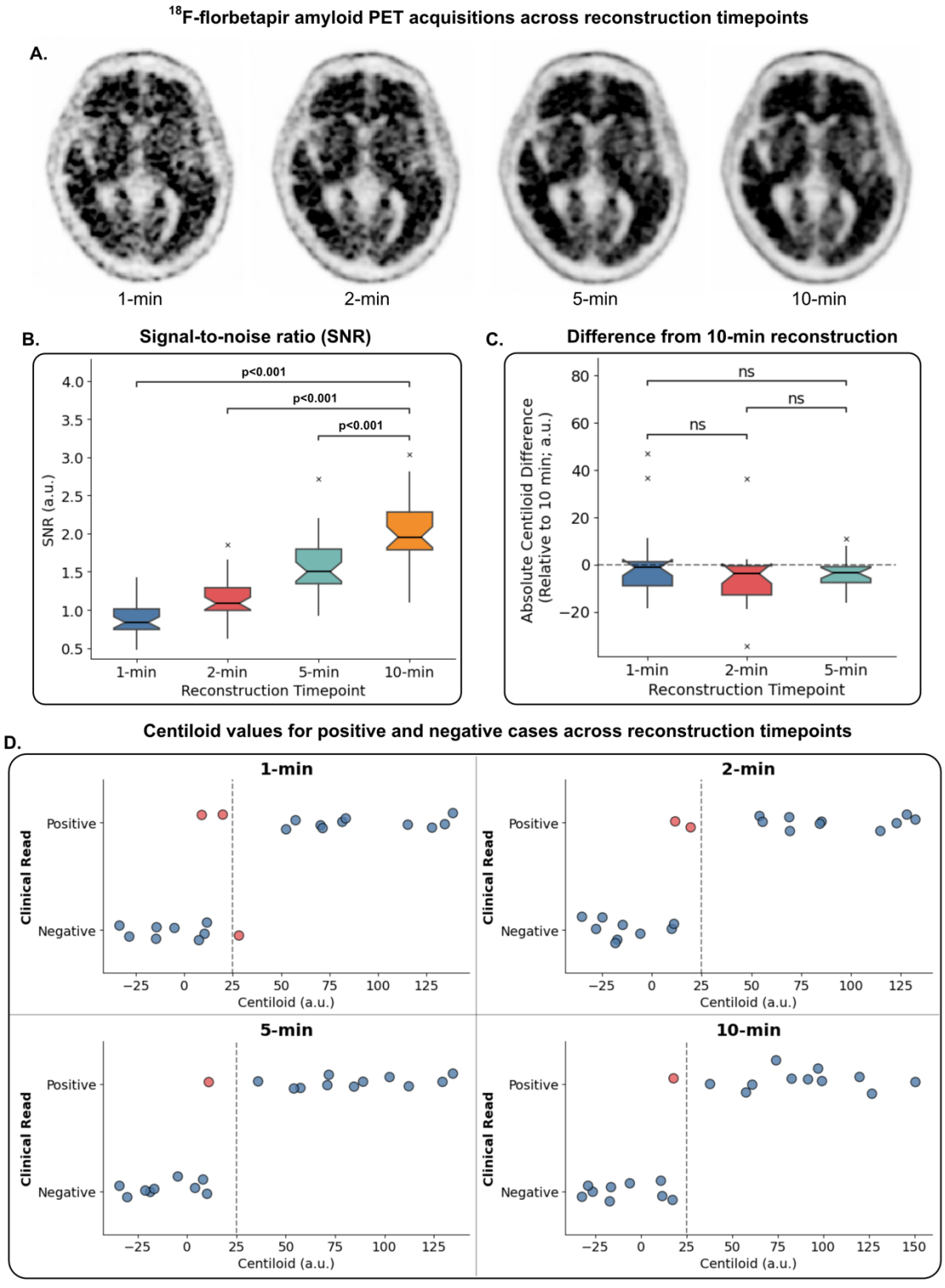

Figure 1: Panel A. representative axial slice for the same subject reconstructed at 1, 2, 5 and 10-minutes. **Panel B.** signal-to-noise ratio (SNR) across all subjects for the reconstructions. **Panel C.** difference between centiloid (CL) score estimated for the 1, 2, and 5-minute reconstructions versus the 10-minute reconstruction. **Panel D.** CL score for all subjects grouped by clinical read. Blue dots represent a match between clinical read and CL threshold, red dots represent a mismatch. The dashed line represents a CL value of 25. n.s. indicates p>0.05

POSTER #11

Multifocal FDG-Avid Osseous Sarcoidosis on PET/CT: An Interesting Case Presentation

Nicholas Campo, MD[1], William Y. Raynor, MD[1], Stephen J. Sozio, DO, MBS[1], Levi Sokol, MD[1], Anthony Yudd MD, PhD, FACR[1], Jeffrey Kempf MD, FACR[1]

1. Department of Radiology, Rutgers Health, Robert Wood Johnson Medical School, New Brunswick, NJ, USA.

Background: Sarcoidosis is a systemic granulomatous disorder of unclear etiology that most commonly affects the lungs but can involve virtually any organ. Extrapulmonary involvement is increasingly recognized, though osseous disease is uncommon and often clinically silent.[1] The prevalence of osseous involvement in sarcoidosis has historically been estimated to be 3-5% though recent literature suggests that the prevalence is closer to 14-18%.[2,3,4] ^{18}F-fluorodeoxyglucose (FDG) PET/CT is a sensitive tool for detecting metabolically active osseous sarcoidosis.[5] We present an interesting case of an asymptomatic patient with sarcoidosis undergoing FDG PET/CT who was found to have extensive osseous involvement.

Methods and Results: A 54-year-old male with sarcoidosis diagnosed two years earlier by endobronchial mediastinal lymph node biopsy, now presenting to the emergency department with nausea and vomiting. He had an elevated erythrocyte sedimentation rate of 52 mm/hr. A CT of the abdomen and pelvis was performed which demonstrated numerous lesions throughout the liver and spleen, as well as retroperitoneal, mediastinal and inguinal lymphadenopathy, which were new compared to a CT scan performed two years prior. Given the extensive adenopathy, the patient was subsequently seen by medical oncology and underwent PET/CT a month later. This study demonstrated multifocal regions of abnormal FDG uptake throughout the body, including extensive lymphadenopathy throughout the chest, abdomen, and pelvis as well as extensive osseous involvement, including, for example, the left humerus (SUV 5.8), right manubrium (SUV 3.6), L3 vertebral body (SUV 4.4), and midline sacrum (SUV 3.5). The patient was asymptomatic at this time and had no bone pain. Approximately a month later, the patient underwent a left inguinal lymph node biopsy, which revealed multifocal non-necrotizing granulomas consistent with sarcoidosis. A repeat FDG PET/CT was performed five months after the baseline FDG PET/CT. This showed markedly increased FDG uptake in the previously noted lymphadenopathy and significant progression of the multiple osseous lesions, including in the left humerus (SUV 7.3), right humerus (SUV 6.9), and midline sacrum (SUV 7.3). A new lesion was identified within the right femoral neck (SUV 4.8). The patient, however, has remained asymptomatic and currently has not been started on therapy.

Discussion: Recent studies have shown that osseous involvement in sarcoidosis, though traditionally considered rare, may be more common when evaluated with FDG PET/CT.[3] These lesions typically involve the axial skeleton and frequently lack corresponding CT abnormalities, highlighting the superior sensitivity of PET/CT for detecting active bone disease.[3,4] The prognosis of osseous sarcoidosis is radiologically and clinically favorable, though no consensus exists for when to initiate treatment for osseous manifestations.[6] Treatment is typically symptom driven, and therapeutic options include hydroxychloroquine, methotrexate, corticosteroids, and infliximab.[5] In treated patients, favorable PET/CT changes were associated with significant

improvements in bone pain.[6] FDG PET/CT not only allows identification of asymptomatic lesions but also provides a baseline for monitoring disease progression or response to therapy.[3,4,6]

Conclusions: This case illustrates the ability of FDG PET/CT to identify asymptomatic osseous sarcoid involvement. The growing identification of these cases with the advent of FDG PET/CT indicates that skeletal involvement is more prevalent than historically appreciated and has meaningful implications for follow-up and treatment decisions.

References

1. Sève P, Pacheco Y, Durupt F, Jamilloux Y, Gerfaud-Valentin M, Isaac S, Boussel L, Calender A, Androdias G, Valeyre D, El Jammal T. Sarcoidosis: A Clinical Overview from Symptoms to Diagnosis. Cells. 2021 Mar 31;10(4):766. doi: 10.3390/cells10040766. PMID: 33807303; PMCID: PMC8066110.
2. Mostard RL, Prompers L, Weijers RE, van Kroonenburgh MJ, Wijnen PA, Geusens PP, Drent M. F-18 FDG PET/CT for detecting bone and bone marrow involvement in sarcoidosis patients. Clin Nucl Med. 2012 Jan;37(1):21-5. doi: 10.1097/RLU.0b013e3182335f9b. PMID: 22157023.
3. Bouchut A, Lhote R, Maksud P, Ben Salem T, Fustier A, Moyon Q, Haroche J, Soussan M, Mathian A, Hie M, Amoura Z, Cohen Aubart F. Prognostic value of hypermetabolic bone sarcoidosis observed by 18F-fluorodeoxyglucose positron emission tomography. Rheumatology (Oxford). 2025 Feb 1;64(2):607-613. doi: 10.1093/rheumatology/keae019. PMID: 38244563.
4. Demaria L, Borie R, Benali K, Piekarski E, Goossens J, Palazzo E, Forien M, Dieudé P, Crestani B, Ottaviani S. 18F-FDG PET/CT in bone sarcoidosis: an observational study. Clin Rheumatol. 2020 Sep;39(9):2727-2734. doi: 10.1007/s10067-020-05022-6. Epub 2020 Mar 20. PMID: 32198555.
5. Akaike G, Itani M, Shah H, Ahuja J, Yilmaz Gunes B, Assaker R, Behnia F. PET/CT in the Diagnosis and Workup of Sarcoidosis: Focus on Atypical Manifestations. Radiographics. 2018 Sep-Oct;38(5):1536-1549. doi: 10.1148/rg.2018180053. Epub 2018 Aug 17. PMID: 30118393.
6. Challal S, Riviere E, Lanseur B, Jeny F, Nunes H, Soussan M, Boissier MC, Semerano L, Saidenberg-Kermanac'h N. Axial bone involvement in sarcoidosis has a good prognosis: Longitudinal study of a cohort of 48 patients. Semin Arthritis Rheum. 2025 Apr;71:152654. doi: 10.1016/j.semarthrit.2025.152654. Epub 2025 Feb 5. PMID: 39951828.

POSTER #12

Toward a Virtual Biopsy for Indeterminate Renal Masses: Multiparametric Contrast-Enhanced Ultrasound and Tc-99m Sestamibi SPECT Case Series

Authors: Louis Mazzarelli MD[1], Kevin Hricko MS MPH[2], Joseph Brito MD[3], Timothy Tran MD[3], Alexander Mazzarelli[4], Richard G. Barr MD[5]

Institutions: [1]Department of Radiology, Lawrence and Memorial and Westerly Hospitals, Yale New Haven Health; [2]University of Connecticut School of Medicine; [3]Department of Urology, Lawrence and Memorial and Westerly Hospitals, Yale New Haven Health; [4]The Williams School; [5]Northeast Ohio Medical University and Southwoods Imaging

Contact: Louis Mazzarelli MD (mazzarellilouis@gmail.com)

Background

Indeterminate renal masses present diagnostic challenges. Percutaneous biopsy carries procedural risks and may yield nondiagnostic results, while observation can delay treatment of clinically significant malignancy. Approximately 25% of patients undergoing surgery for suspected renal malignancy have benign tumors, highlighting the need for improved preoperative characterization. Advanced molecular imaging such as carbonic anhydrase IX (CAIX)-targeted PET shows promise for clear cell RCC detection but is not yet FDA-approved or widely available. Multiparametric contrast-enhanced ultrasound (mpCEUS) and Tc-99m sestamibi SPECT may provide an accessible noninvasive 'virtual biopsy,' combining vascular and metabolic information to guide management decisions including observation, cryoablation, or surgery.

Methods

We retrospectively reviewed eight renal lesions in seven patients evaluated with multiparametric CEUS. CEUS included high-resolution B-mode, color Doppler, microvascular flow, dynamic contrast acquisitions, bubble-destruction/replenishment, super-resolution post-processing, and time-of-arrival analysis. Oncocytoma was suspected on CEUS when lesions demonstrated: (1) co-temporal contrast arrival with adjacent cortex, (2) homogeneous enhancement, (3) well-circumscribed borders, (4) isoechoic or hypoechoic appearance on grayscale, and (5) organized radial or spoke-wheel vascularity on super-resolution imaging. Cases with CEUS features suggesting oncocytoma or indeterminate patterns underwent Tc-99m sestamibi SPECT to assess metabolic activity. Avid sestamibi uptake (indicating high mitochondrial content) supported

oncocytoma, while photopenic uptake suggested non-oncocytic neoplasms such as clear cell RCC. A single radiologist (Louis Mazzarelli, LM) interpreted all CEUS and SPECT studies. Imaging findings were correlated with biopsy, histology, or follow-up.

Results

Results

Eight lesions were evaluated: five oncocytomas, two clear cell RCCs, and one pending confirmation. CEUS alone correctly classified 5/8 lesions (62.5%). Three cases showed CEUS-SPECT discordance. Two oncocytomas demonstrated avid peripheral uptake with central photopenia on SPECT, correlating with central scarring characteristic of oncocytoma. In two lesions (same patient), CEUS favored oncocytoma, but SPECT demonstrated photopenic uptake throughout, prompting biopsy that confirmed clear cell RCC; the patient underwent successful cryoablation. A third case (CEUS favoring oncocytoma, SPECT photopenic) is scheduled for biopsy with management directed toward partial nephrectomy or ablation. CEUS+SPECT integration achieved 87.5% accuracy (7/8 cases correctly classified or appropriately triaged). SPECT identified all three discordant cases where CEUS alone would have misclassified malignancy as benign.

Table 1. CEUS-SPECT Integration Results

Case	Size (cm)	CEUS Impression	SPECT Uptake	Final Diagnosis	Concordance
1	3.5	Oncocytoma	Photopenic	Pending	Discordant
2	5.3	Oncocytoma	Avid	Oncocytoma	Concordant
3	1.8	Oncocytoma	Avid	Oncocytoma	Concordant
4	2.9	Oncocytoma	Avid	Oncocytoma	Concordant
5	2.1	Oncocytoma	Avid (Central Photopenia)	Oncocytoma	Concordant
6	4.6	Oncocytoma	Avid (Central Photopenia)	Oncocytoma	Concordant
7	1.7	Oncocytoma	Photopenic	Clear cell RCC	Discordant
8	2.4	Oncocytoma	Photopenic	Clear cell RCC	Discordant

Conclusion

This case series demonstrates the feasibility of integrating multiparametric CEUS with Tc-99m sestamibi SPECT as a noninvasive virtual biopsy for renal masses. CEUS provides detailed vascular mapping, but SPECT adds critical metabolic information that prevented misclassification of malignancy. Combined CEUS+SPECT improved diagnostic accuracy from 62.5% to 87.5%. SPECT reclassified two CEUS-presumed oncocytomas as clear cell RCC,

leading to appropriate biopsy and cryoablation, and identified a third discordant lesion triaged for surgical intervention. Although tissue diagnosis was obtained in all cases to validate imaging findings, these results support CEUS-SPECT integration to reduce unnecessary biopsies when concordant while directing discordant cases to tissue confirmation. Larger multi-reader studies are warranted to validate this virtual biopsy paradigm.

FIGURES

Figure 1: Oncocytoma

mpCEUS shows organized radial vasculature with homogeneous enhancement pattern. Sestamibi SPECT demonstrates avid homogeneous uptake throughout the lesion (arrows), correctly identifying benign oncocytoma. The concordant benign features on both modalities supported observation without immediate intervention.

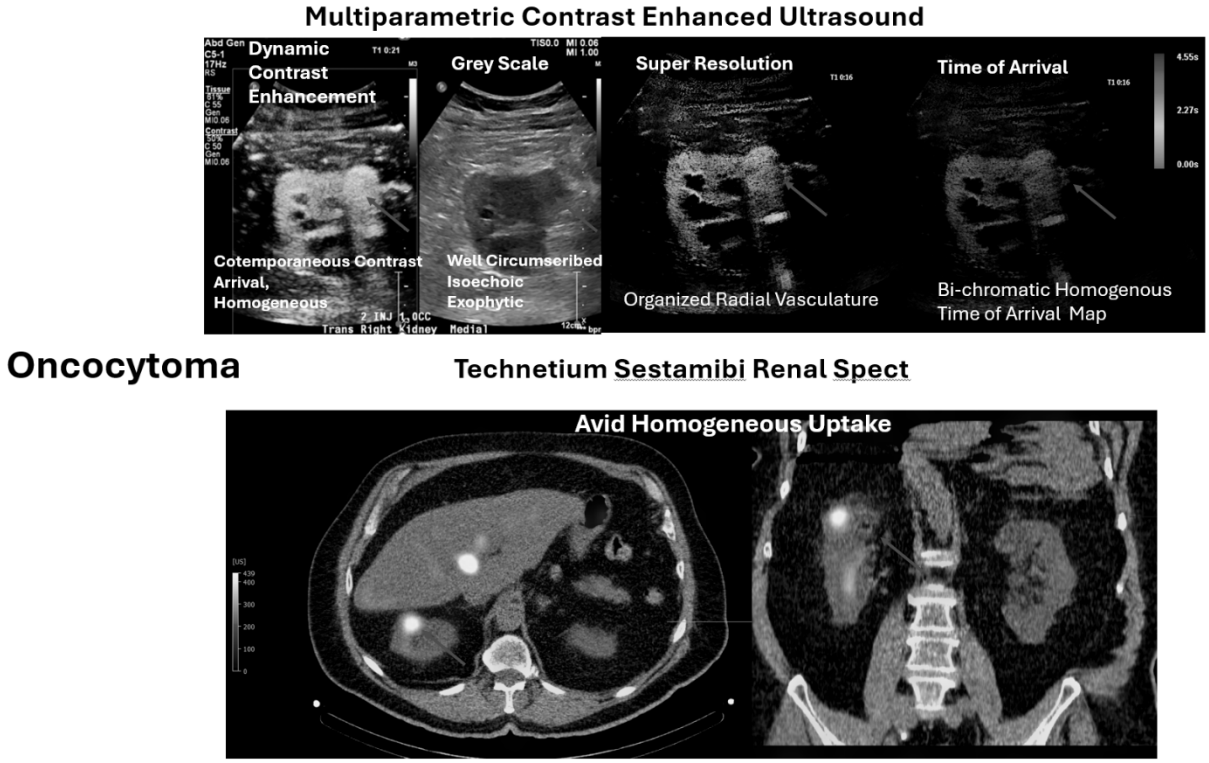

Figure 2: Clear Cell Renal Cell Carcinoma

mpCEUS demonstrates disorganized irregular vasculature with perfusion defects (arrows). Sestamibi SPECT shows absent uptake in the lesion, correctly identifying malignancy. This multiparametric approach prevented misclassification and led to appropriate tissue diagnosis followed by successful cryoablation.

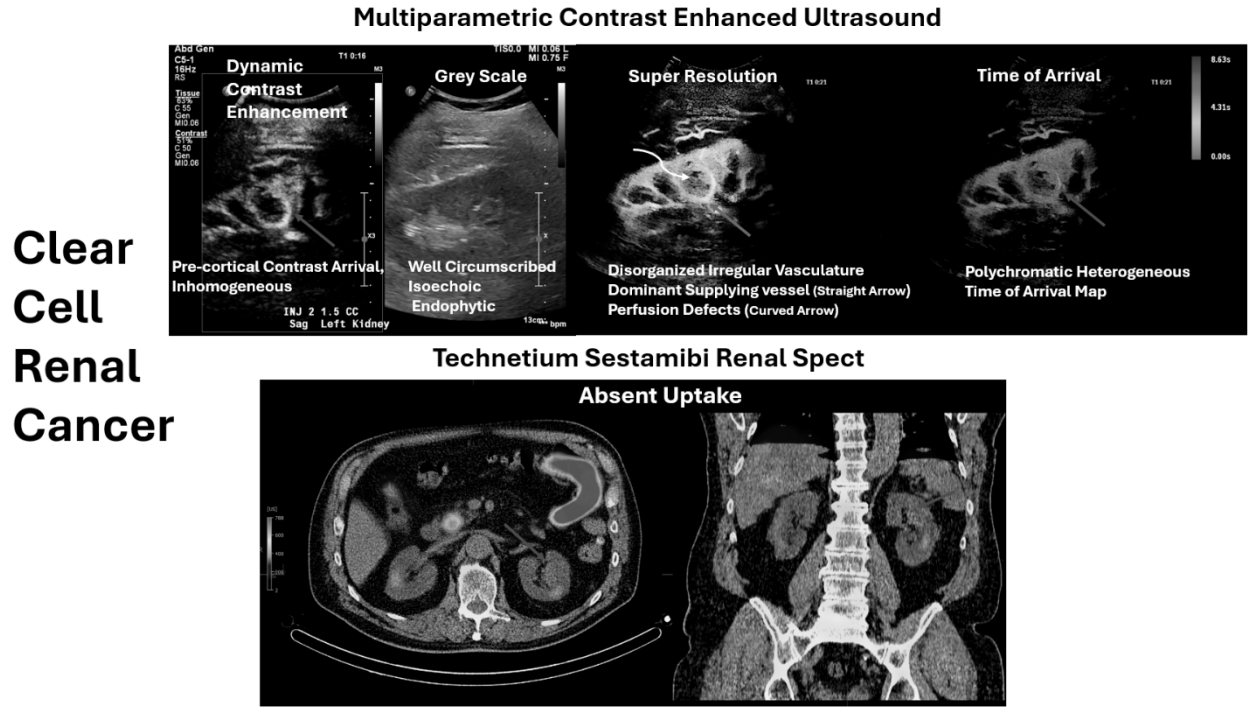

POSTER #13

Lymphoscintigraphic Evaluation of Postoperative Lymphocele: Educational Insights from a Case Study

Authors: Alireza Mohseni, Shazia Naseem, Siddarth Ragupathi, Kwang Chun, Ana Valdivia

Department of Radiology, Division of Nuclear Medicine, Montefiore Medical Center/Albert Einstein College of Medicine, Bronx, NY

Background

The lymphatic system transports large molecules into the vascular circulation and can be evaluated using several imaging modalities, including conventional lymphography, MR lymphography, contrast-enhanced ultrasound, near-infrared fluorescence imaging, and lymphoscintigraphy (1). Lymphoscintigraphy is a simple, noninvasive, and well-established technique that has been used for decades to image the lymphatic system function (2,3).

Methods

Lymphoscintigraphy is performed following intradermal injection of 0.5–1.0 mCi Tc-99m filtered sulfur colloid into the interdigital spaces of both feet. Dynamic and delayed planar images are acquired to evaluate lymphatic transport from the lower extremities to the inguinal and pelvic regions. If needed, SPECT/CT is performed for precise anatomic localization of radiotracer accumulation (4).

Results

An 83-year-old male who had recently undergone robotic bilateral inguinal hernia repair developed a large palpable preperitoneal mass. The differential diagnosis included seroma, lymphocele, and hematoma. Lymphoscintigraphy demonstrated sluggish bilateral lymphatic flow from the feet with progressive tracer accumulation in the lower abdomen, localized to the preperitoneal collection. Delayed imaging confirmed radiotracer retention within the cavity and drainage tubing, consistent with an active lymphatic leak. SPECT/CT confirmed focal uptake within the preperitoneal space, supporting the diagnosis of a postoperative lymphocele.
MRI correlated with a large cystic collection in the same region. Interventional radiology initially recommended lymphatic embolization; however, the surgical team elected for a less invasive approach. The patient underwent targeted surgical repair with patching of leakage sites, resulting in resolution of the lymphocele and no recurrence on follow-up.

The pattern of radiotracer accumulation was analogous to prior reports of lymphoscintigraphic visualization of lymphatic leakage in other postoperative settings, such as chylothorax reported by Bybel et al. (5). Both cases demonstrate the value of lymphoscintigraphy in detecting active lymphatic communication with abnormal fluid collections.

Conclusion

Lymphoscintigraphy is a valuable diagnostic tool for identifying postoperative lymphatic leaks and confirming the lymphatic origin of fluid collections. The integration of functional imaging with SPECT/CT localization enables accurate diagnosis, guides surgical or conservative management, and aids postoperative follow-up.

References:

1. Munn LL, Padera TP. Imaging the lymphatic system. Microvasc Res. 2014;96:55–63. doi: 10.1016/j.mvr.2014.06.006
2. Weissleder R, Thrall JH. The lymphatic system: Diagnostic imaging studies. Radiology. 1989;172:315–7. doi: 10.1148/radiology.172.2.2748809.
3. Villa G, Campisi CC, Ryan M, Boccardo F, Di Summa P, Frascio M, et al. Procedural recommendations for lymphoscintigraphy in the diagnosis of peripheral lymphedema: The genoa protocol. Nucl Med Mol Imaging. 2019;53:47–56. doi: 10.1007/s13139-018-0565-2.
4. Ranzenberger LR, Pai RB. Lymphoscintigraphy. [Updated 2024 Mar 6]. In: StatPearls [Internet]. Treasure Island (FL): StatPearls Publishing; 2025 Jan-. Available from: https://www.ncbi.nlm.nih.gov/books/NBK563213/
5. Bybel B, Neumann DR, Kim BY, Amin K, Rice T. Lymphoscintigraphy using (99m)Tc filtered sulfur colloid in chylothorax: a case report. J Nucl Med Technol. 2001 Mar;29(1):30-1. PMID: 11283214.

POSTER #14

Implementing Post-Therapy PSMA Imaging in a Multidisciplinary Theranostics Clinic

Nina Le, MD, Christopher Caravella, LNMT, Baho Sidiqi, MD, Clary Evans, MD, Josephine Rini, MD

Background: Pluvicto (lutetium Lu-177 vipivotide tetraxetan) is an FDA-approved, PSMA-targeting radioligand therapy (RLT) that delivers beta radiation to PSMA-expressing cells. Initially approved in March 2022 for PSMA-positive metastatic castration-resistant prostate cancer after androgen receptor pathway inhibition and taxane chemotherapy, the indication expanded in March 2025 to include chemotherapy-naïve patients. Randomized trials show that PSMA RLT prolongs survival, improves quality of life, and lowers PSA levels. Gamma emissions (~113 and 208 keV) from Lu-177 enable post-therapy imaging with SPECT/CT and planar whole-body (WB) imaging. Post-therapy imaging may be useful to verify radiopharmaceutical delivery, detect extravasation, identify new sites of disease, reveal nontarget uptake, compare lesions across cycles, and occasionally to uncover lesions overlooked on PSMA PET/CT. Post-therapy imaging may inform treatment decisions and support dosimetry. Despite growing interest, reproducible outpatient workflows, billing pathways, and operational lessons remain limited. We describe a reproducible workflow for post-therapy PSMA imaging in an outpatient multidisciplinary theranostics clinic and show case illustrations.

Methods: Post-therapy PSMA imaging (SPECT/CT and WB) was implemented with a standardized cadence: PSMA RLT administration on Friday in Radiation Medicine and imaging ~72-96 hours later in Radiology. Imaging time-points were selected to optimize count statistics, staff coverage, and scanner utilization while minimizing staff radiation exposure.

Imaging protocol/calibration: Siemens Biograph Intevo Bold peaked for Lu-177 at 113/208 keV. Initially, planar and SPECT acquisitions used dual photopeaks (113/208 keV). After initiating quantitation, SPECT used only 208 keV per vendor guidance, while planar remained at dual peak. Medium energy low penetration collimators were used.

At 72-96 hours following PSMA RLT, patients underwent vertex-to-knee (V-K) planar WB imaging followed by V-K multibed SPECT/CT. Voiding was encouraged before/between acquisitions. Total imaging time was ~75 minutes. Datasets were merged with vendor workflows and reconstructed with Flash 3D and xSPECT (CT attenuation, scatter, resolution recovery). Patient weight, administered activity, and administration time were entered to derive quantitative SUVs in xSPECT. WB intensities were standardized for serial comparison.

Discrete radiology orderables ("NM PSMA SPECT/CT" and "NM POST TX PSMA WB IMG") were created. Reimbursement followed SNMMI/ACNM guidance: CPT 78802 (V-K planar) and CPT 78832 (V-K SPECT/CT) billed together in one encounter without separate radiopharmaceutical charges. Prior authorization, not required for Medicare beneficiaries, was pursued for non-Medicare payers.

Results: From February to mid-October 2025, 18 patients were treated with 48 cycles of PSMA RLT. Twenty-six post-therapy PSMA SPECT/CT and WB images were acquired in 13 patients. Imaging was well-tolerated. Payer claims analysis demonstrated consistent reimbursement. Serial posttherapy images illustrating response and progression, and cases where PSMA SPECT/CT identified pleural, adrenal, and hepatic lesions initially overlooked on PSMA PET/CT are presented.

Conclusion: Centers should consider incorporating post-therapy PSMA imaging, as it may help personalize treatment through serial qualitative, and potentially quantitative assessments (including dosimetry). A standardized outpatient post-therapy PSMA imaging program was feasible and operationally efficient within a multidisciplinary theranostics clinic. The workflow enabled imaging at predefined time points, compliant billing, and consistent qualitative and semiquantitative analysis. Our experience offers a practical blueprint to integrate post-therapy PSMA imaging into routine clinical care.

PSMA-Positive Lesions Identified on PSMA-SPECT/CT & Retrospectively seen on PSMA PET/CT

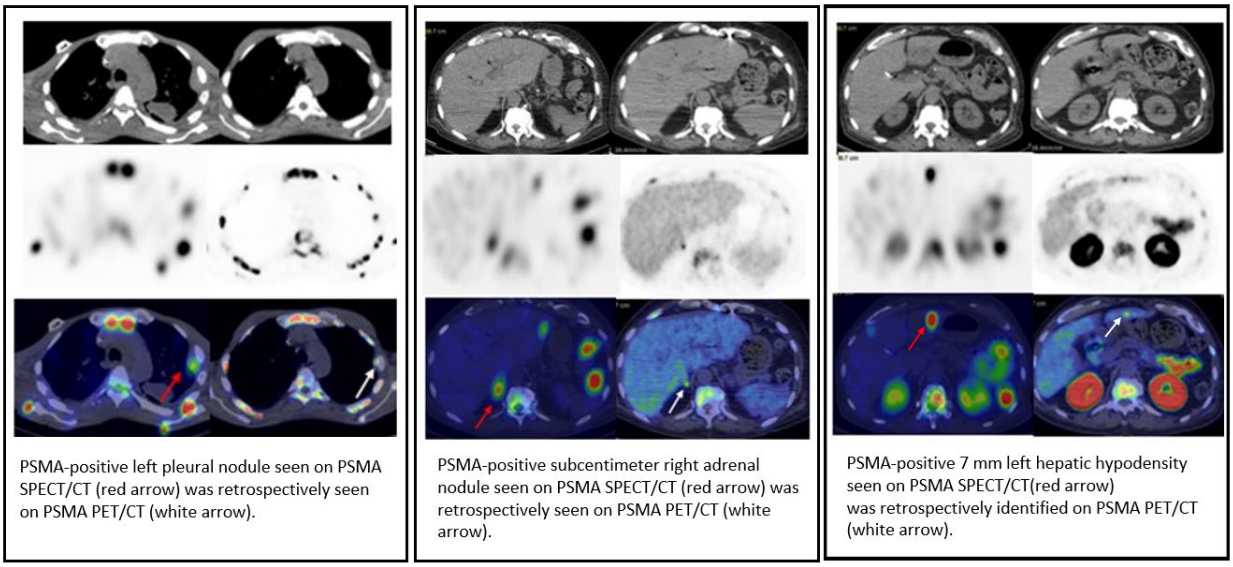

PSMA-positive left pleural nodule seen on PSMA SPECT/CT (red arrow) was retrospectively seen on PSMA PET/CT (white arrow).

PSMA-positive subcentimeter right adrenal nodule seen on PSMA SPECT/CT (red arrow) was retrospectively seen on PSMA PET/CT (white arrow).

PSMA-positive 7 mm left hepatic hypodensity seen on PSMA SPECT/CT(red arrow) was retrospectively identified on PSMA PET/CT (white arrow).

POSTER #15

From Suspicion to Stratification: PET/CT in Pediatric Langerhans Cell Histiocytosis Disease Characterization

Graeme Benzie, MD, MSc[1]; Aram Tonoyan, MD, PhD[1]; Tae-young Roh, BSc[2]; Prasanta Karak, MD[1]

[1]Department of Radiology, Hartford Hospital, Hartford, Connecticut; [2]Frank H. Netter MD School of Medicine, Quinnipiac University.

Introduction:

Langerhans cell histiocytosis (LCH) is a rare myeloproliferative disease that predominantly affects children, with 50% of cases diagnosed before the age of three (Liu *et al.* 2022).

LCH is categorized into two main forms: single-system and multisystem disease. The multisystem form is further stratified based on the involvement of high-risk organs, such as the liver, spleen, and bone marrow.

Single-system LCH has an excellent prognosis, with nearly 100% survival and treatment typically not requiring chemotherapy (Jiang W. *et al.* 2025). Multisystem low-risk LCH is managed with one year of chemotherapy, achieving a 90–99% survival rate. In contrast, multisystem high-risk LCH necessitates more intensive chemotherapy and may require stem cell transplantation, with a 5-year survival rate of 75–85% (Thalhammer *et al.* 2025).

F-18-FDG PET/CT is the imaging modality of choice for the initial staging of pediatric LCH, given its superior ability to detect active lesions, as recommended by the NCCN Clinical Practice Guidelines in Oncology for Histiocytic Neoplasms (NCCN, Version 2.2021). PET/CT is also valuable for detecting recurrence of metabolically active disease following chemotherapy.

Objective:

To examine the role of PET/CT in pediatric LCH imaging through a series of illustrative clinical cases.

Case Presentations/Findings

Case 1: A 9-year-old female presented with a two-month history of lower back pain. Initial spinal radiography revealed partial collapse of the L4 vertebral body. Follow-up MRI confirmed the collapse but was inconclusive in distinguishing between a possible traumatic or neoplastic etiology. A CT-guided biopsy of the L4 lesion subsequently confirmed LCH. F-18-FDG PET/CT performed for staging revealed additional hypermetabolic lesions in the C4 pedicle and lamina, L4 vertebral body, and right superior pubic tubercle, establishing the diagnosis of single-system multifocal LCH.

Case 2: A 3½-year-old female presented with a one-week history of right leg pain and limp, initially attributed to a trampoline fall two months earlier. Radiography revealed a 3-cm radiolucent lesion in the proximal right tibia. A skeletal survey demonstrated a second similar lesion in the left parietal bone. MRI of the tibia showed an expansile bone lesion, which was biopsied and confirmed as LCH. One week later, the patient developed eye pain. MRI of the brain redemonstrated the left parietal lytic lesion and revealed erosive changes in the right frontal sinus. 18F-FDG PET/CT demonstrated avid radiotracer uptake in the right tibial and left parietal lesions, with no abnormal uptake in the right frontal sinus. These findings established the diagnosis of single-system multifocal LCH.

Discussion/Conclusion:

These cases underscore the clinical value and diagnostic precision of F-18-FDG PET/CT in pediatric Langerhans cell histiocytosis. Beyond its established indications in initial staging and surveillance for disease recurrence, PET/CT demonstrated superiority over conventional imaging in lesion characterization and disease stratification. In one case, a lesion initially presumed to be unifocal was reclassified as multifocal single-system disease based on additional hypermetabolic foci. In a second case, PET/CT accurately delineated two metabolically active bony lesions and excluded right frontal sinus involvement, thereby confirming suspected multifocal involvement of the CNS and refining the diagnosis to single-system multifocal disease.

References:

Liu H, Stiller CA, Crooks CJ, et al. *Incidence, prevalence and survival in patients with Langerhans cell histiocytosis: a national registry study from England, 2013–2019.* **Br J Haematol.** 2022;199(5):728–738. doi:10.1111/bjh.18459

Thalhammer J, Jeziorski E, Marec-Bérard P, et al.; French LCH Working Group. *Childhood Langerhans cell histiocytosis hematological involvement: severity associated with BRAFV600E loads.* **Blood.** 2025;145(10):1061–1073. doi:10.1182/blood.2024025625

National Comprehensive Cancer Network. *NCCN Clinical Practice Guidelines in Oncology: Histiocytic Neoplasms, Version 2.2021*. J Natl Compr Canc Netw. 2021;19(11):1277-1303. Accessible at: https://www.erdheim-chester.org/wp-content/uploads/2022/08/NCCN-Guidelines-for-Histiocytic-Neoplasms.pdf.

POSTER #16

Expanding Applications of PET/CT in Pediatrics: From Oncology to Neurology

Muhammad Awais Ashraf, D.O.
Radiology Resident, R4
muhammad.a.ashraf90@gmail.com
Hartford Hospital

Veronica Periera, M.D.
Radiology Resident, R3
vmp823@gmail.com
Hartford Hospital

Prasanta Karak, M.D.
Attending Physician
Prasanta.Karak@hhchealth.org
Hartford Hospital, Jefferson Radiology

Background

Positron Emission Tomography combined with Computed Tomography (PET/CT) is well established in adult imaging. Its role in pediatrics is rapidly growing, driven by advances in technology and increasing clinical experience.

Objective

To highlight the expanding clinical applications of PET/CT in pediatric imaging through illustrative real-world cases spanning established and emerging indications.

Methods

We reviewed seven pediatric cases across oncologic, inflammatory/histiocytic, benign osseous, neuroendocrine, and metabolic neurologic presentations. For each, we assessed how PET/CT informed diagnosis, staging, treatment response, or management, with attention to tracer selection and correlation with CT and MRI.

Cases

Burkitt lymphoma: Baseline PET/CT demonstrated widespread nodal, splenic, and colonic hypermetabolism with indeterminate marrow uptake. Follow-up showed complete metabolic response of nodal disease (Fig 1).

Soft-tissue sarcoma: Intense uptake in a primary thigh mass with a satellite nodule, plus a hypermetabolic abdominal-wall focus, acetabular osseous involvement, and multiple bilateral hypermetabolic pulmonary metastases. Photopenic cortical defects on PET prompted urgent brain MRI, which confirmed multiple intracranial metastases (Fig 2).

Ewing sarcoma: Large right hemithoracic mass with lower-than-expected avidity; interval PET/CT showed decreased size and activity. After resection, a small indeterminate surgical-bed focus was seen and subsequently resolved on follow-up (Fig 3).

Langerhans cell histiocytosis: An avid expansile lesion in the proximal right tibia with additional multifocal activity decreased on therapy. Later studies showed faint residual tibial uptake and benign-appearing soft-tissue activity; calvarial lesions on CT demonstrated progressive healing, with metabolic assessment limited near the brain (Fig 4).

Fibrous dysplasia: Polyostotic involvement of the craniofacial skeleton, ribs/extremities, pelvis, and proximal femora with variable FDG uptake and characteristic ground-glass changes on CT in a patient with McCune-Albright syndrome and high skeletal burden (Fig 5).

Paraganglioma vs. schwannoma: ^{68}Ga-DOTATATE PET/CTperformed to differentiate a carotid-space mass. A solitary, intensely receptor-avid skull-base lesion corresponded to an enhancing mass on MRI, compatible with paraganglioma (Fig 6).

Epilepsy metabolic evaluation:

• ***Case A*:** Mild asymmetric hypometabolism in the right high parietal/posterior occipital cortex with possible superior posterior frontal involvement, concordant with MRI-demonstrated atrophy/gliosis; no additional definite epileptogenic focus (Fig 7).

• ***Case B*:** Despite diffuse cortical suppression from general anesthesia during uptake, focal decreased metabolism was identified in the right mesial temporal lobe and the anteromedial left frontal lobe (Fig 7).

Conclusion

PET/CT is increasingly vital in pediatric imaging. These cases demonstrate its growing importance in defining disease extent, monitoring treatment response, refining differential diagnoses, and localizing potential epileptogenic zones, supporting broader understanding and careful implementation in pediatric practice.

POSTER #17

Abstract

Title: "Diagnostic Pitfalls of Cardiac FDG PET/CT in Sarcoidosis: Influence of Inadequate Myocardial Suppression Protocols"

Authors:
Shazia Naseem, MD; Affaf Gul, MD; Alireza Mohseni, MD: Syed Mahmood, MD.
Division of Nuclear Medicine, Department of Radiology
Montefiore Medical Center, The University Hospital for Albert Einstein College of Medicine
Bronx, NY 10461
Emails: snaseem@montefiore.org; agul@montefiore.org; amohseni@montefiore.org; syemahmood@montefiore.org

Background:
Sarcoidosis is a systemic, inflammatory disease affecting multiple organs, including the lungs and heart. Cardiac 18F-fluorodeoxyglucose (FDG) PET/CT is used not only for early disease detection, but also for therapy monitoring and image guided biopsy. The pattern of patchy focal uptake and mismatched defects is suggestive of cardiac sarcoidosis (CS); diffuse and heterogeneous pattern especially in basal and lateral wall suggests inadequate myocardial uptake suppression. SUVmax high values often reflect inflammation and must be interpreted within a clinical context. The accuracy of FDG PET/CT depends heavily on suppression of physiological myocardial glucose metabolism by following specific dietary and fasting protocols.

Methods:
This case series includes patients at Albert Einstein College of Medicine/Montefiore Medical Center with suspected cardiac sarcoidosis who underwent cardiac FDG PET/CT, along with a Rubidium-82 (Rb-82) Myocardial Perfusion Rest only study, from October 15, 2024, to October 15, 2025. Patients were instructed to follow a structured patient preparation protocol as recommended by the joint SNMMI/ASNC expert consensus document, by fasting for 12 hours, and following a high-fat and low-carbohydrate diet for at least 24 hours. Adequate myocardial suppression was defined as either no visible myocardial FDG uptake or uptake lower than that of the blood pool.

Results:
Of 49 patients, ten demonstrated inadequate patient preparation; and the following five representative cases illustrate unexpected uptake patterns associated with suboptimal preparation.

Case 1: A 48-year-old man with nonischemic cardiomyopathy exhibited diffuse myocardial uptake with superimposed focal activity above background in the anterior and anterolateral walls, and mid lateral wall (SUVmax 5.9), producing a *focal-on-diffuse* pattern. Perfusion imaging revealed a large defect in the inferolateral and septal regions. The results were non-diagnostic for assessment of potential cardiac inflammation from active cardiac sarcoidosis. No tracer uptake was appreciated in the thoracic lymph nodes. There was a metabolic mismatch in the perfusion defect area due to inadequate preparation.

Case 2: A 54-year-old woman with complete heart block and prior evidence of sarcoidosis on MRI demonstrated diffuse myocardial tracer uptake with areas of *focal increased activity* corresponding

to perfusion defects in mid-distal anterior/anteroseptal wall, septum (SUVmax 19.4, prior 11.2) indicating possible localized inflammation in region of myocardial damage. Mismatch is seen in anteroseptal wall. No metabolic tracer uptake was seen in chest nodes.

Case 3: A 60-year-old man with coronary artery disease and conduction disturbances demonstrated diffusely increased myocardial uptake despite prior focal findings. Uptake was *heterogeneous* in mid to distal anterior/anterolateral extending to mid to basal anterior septum, mid to basal inferior wall extending to basal inferior septum (SUVmax 14, prior 9.3) and the amount of myocardium with SUVmax >4 was 318cc vs 250cc in prior. No uptake was seen in thoracic lymph nodes.

Case 4: A 63-year-old man with non-ischemic cardiomyopathy and MRI showing multiple areas of enhancement in non-coronary distribution. FDG showed mild diffuse uptake throughout myocardium, most prominent in *basal inferoseptal area (SUVmax 2.8), that is lower than that of blood pool* conferring a low probability for cardiac inflammation from active sarcoidosis. Perfusion images show defects in mid to distal lateral wall, likely fibrogranulomatous replacement from chronic sarcoidosis. No tracer uptake was seen in thoracic nodes.

Conclusion:
Inadequate patient preparation affects FDG PET/CT image interpretation for sarcoidosis. Adherence to standardized preparation protocols, including a high-fat, low-carbohydrate diet, prolonged fasting, is essential to suppress physiological myocardial activity. SUVmax is not a reliable indicator; however, SUVmax can be useful in active inflammation and must be interpreted with clinical context.

References:

1. Chareonthaitawee P, Beanlands RS, Chen W, et al. Joint SNMMI–ASNC expert consensus document on the role of 18F-FDG PET/CT in cardiac sarcoid detection and therapy monitoring. *J Nucl Med.* 2017;58(8):1341-1353. doi:10.2967/jnumed.117.196287
2. Osborne MT, Hulten EA, Murthy VL, et al. Patient preparation for cardiac fluorine-18 fluorodeoxyglucose positron emission tomography imaging of inflammation. *J Nucl Cardiol.* 2017;24(1):86-99. doi:10.1007/s12350-016-0551-6
3. Chan SH, Huang CK, Luzhbin D, Hou PN, Chang YT, Wu J. Meta-analysis of the effectiveness of heparin in suppressing physiological myocardial FDG uptake in PET/CT. J Nucl Cardiol. 2023;30(6):2454-2463. doi:10.1007/s12350-022-03149-9
4. Lu Y, Grant C, Xie K, Sweiss NJ. Suppression of myocardial 18F-FDG uptake through prolonged high-fat, high-protein, and very-low-carbohydrate diet before FDG-PET/CT for evaluation of patients with suspected cardiac sarcoidosis. *Clin Nucl Med.* 2017;42(2):88-94. doi:10.1097/RLU.0000000000001462.
5. Kherajani P, Farag AA, Morgan WS, Hage FG, Bhambhvani P. Complete resolution of focal-on-diffuse myocardial activity pattern on FDG PET/CT by prolonging the dietary preparation protocol in cardiac sarcoidosis. *J Nucl Cardiol.* 2023;30(6):2525-2530. doi:10.1007/s12350-022-03167-7

POSTER #18

FDG-PET/CT: A Cornerstone in Diagnosing and Managing Pyogenic Spondylodiscitis - Vertebral Osteomyelitis.

Aram Tonoyan, MD, PhD; Graeme Benzie, MD, MSc; Prasanta Karak, MD

Introduction:
Vertebral osteomyelitis (pyogenic spondylodiscitis) is a potentially disabling condition with a mortality rate of 2–12%, residual functional deficits in 15% of patients. Delayed diagnosis of ≥8 weeks strongly predicts high mortality and morbidity.

Objective:
To review the complex diagnostic approach and highlight the central role of FDG-PET/CT in diagnosis of vertebral osteomyelitis.

Case Presentation/Imaging Findings:
Case 1: A 62-year-old man with a mechanical cardiac valve presented with three weeks of back pain and low-grade fever. CT revealed an abdominal aortic aneurysm (Fig. 1a). FDG-PET/CT, performed for suspected mycotic aneurysm, demonstrated intense uptake in the aneurysm, confirming infection, and in the intervertebral disc and adjacent vertebrae, consistent with vertebral osteomyelitis (Fig. 1b). Blood cultures grew *Proteus*.
Case 2: A 51-year-old man with Diabetes Mellitus type-2 presented with a one-week history of back pain and fever. CT and MRI demonstrated vertebral osteomyelitis (Fig 2a-d). Biopsy grew *Mycobacterium abscessus*. Despite antibiotic therapy, symptoms persisted. FDG-PET/CT showed intense uptake in the affected disc and vertebral bodies, consistent with vertebral osteomyelitis (Fig. 2e).

Discussion/Conclusion:
Vertebral osteomyelitis affects the lumbar (48%), thoracic (35%) and cervical (6.5%) spine. The primary source of infection is bacteremia, direct inoculation and contiguous spread from adjacent infection.

Symptoms are nonspecific - back pain, fever, elevated inflammatory markers - with possible complications such as meningitis, myelitis, spinal cord compression. Because biopsy identifies a pathogen in fewer than 50% of cases, imaging is essential for diagnosis.

MRI has a sensitivity of 96% and specificity of 92%. Key findings include endplate erosions/destruction, contrast enhancement and abnormal signal (low on T1 and high on T2) of the disc, bone marrow, and surrounding soft tissues, as well as loss of disc height, vertebral collapse, and paraspinal/epidural edema or phlegmon/abscess formation. DWI can help distinguish acute vertebral osteomyelitis - characterized by high signal in the infected structures - from chronic disease, which typically demonstrates low signal. Lytic osseous changes are better evaluated on CT.
Limitations of MRI include persistent imaging abnormalities despite clinical improvement, artifacts from spinal hardware, and inability to reliably distinguish early spondylodiscitis from degenerative disk disease.

FDG-PET/CT demonstrates sensitivity and specificity comparable to MRI but superior for early diagnosis when MR is unable, evaluating treatment response and for patients with spinal hardware. Physiologically increased FDG uptake after spine surgery or fracture typically normalizes within 3–4 months.

Gallium-67 citrate scanning has sensitivity and specificity >90% but is less accurate than FDG-PET/CT due to poor spatial resolution and requires a multiday, time-consuming protocol compared with FDG-PET/CT.

Other nuclear medicine techniques (Tc-99m MDP bone scintigraphy, WBC scintigraphy) have lower sensitivity and specificity and are not useful for diagnosing vertebral osteomyelitis.

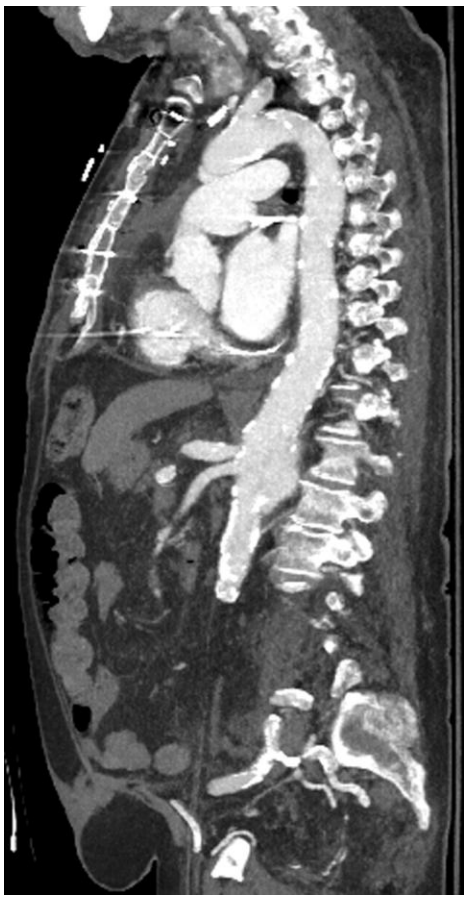

Fig. 1. (a) Contrast-enhanced CT; (b) FDG-PET/CT

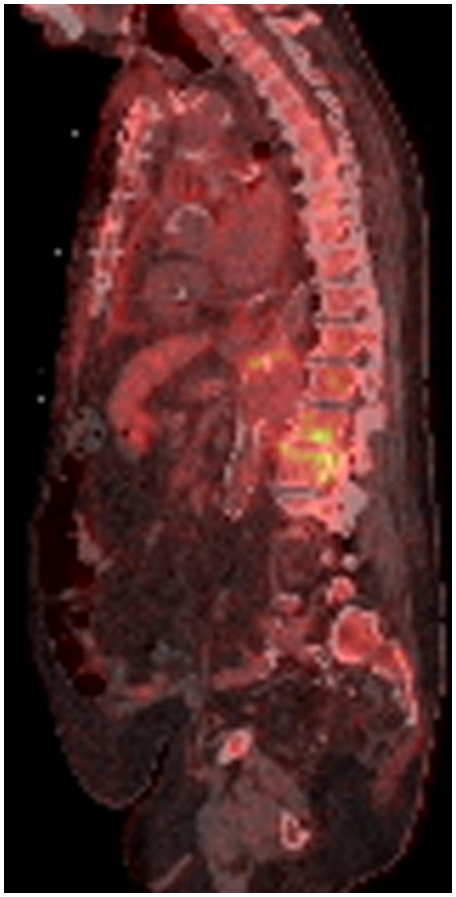

Fig. 2. (a) CT; (b) T1; (c) contrast-enhanced T1; (d) T2 with fat saturation; (e) FDG-PET/CT

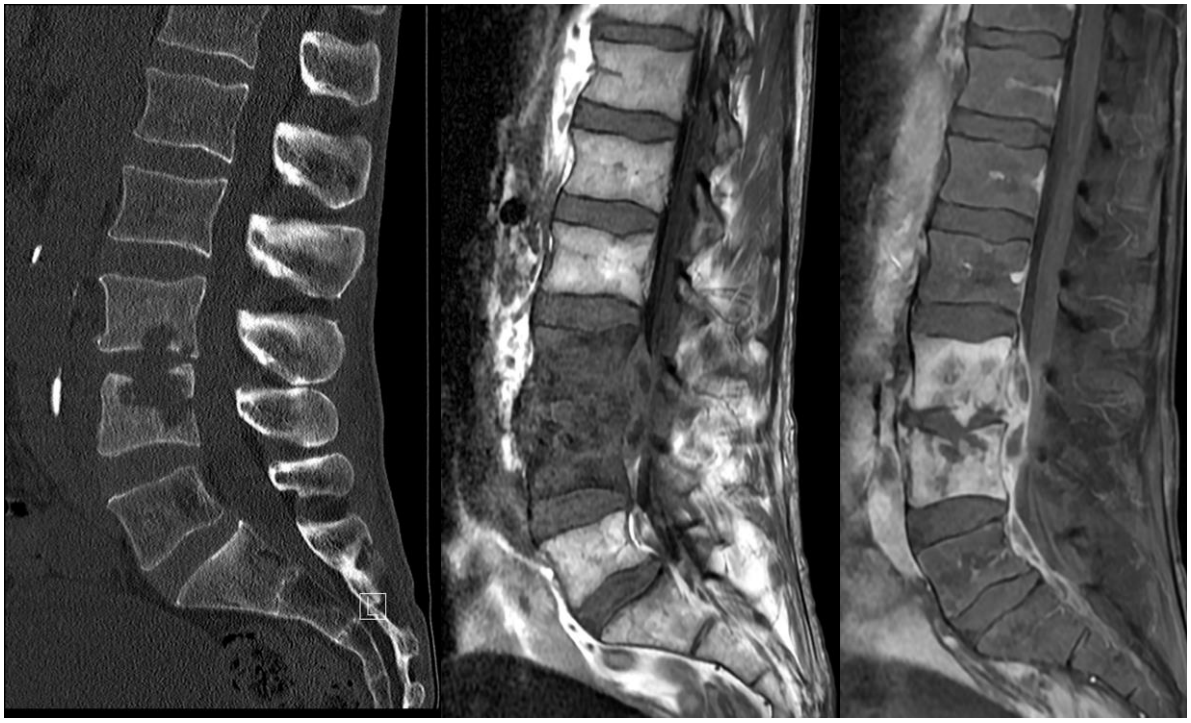

POSTER #19

Abstract

Title:

Facilitating Artificial Intelligence Education in Nuclear Medicine: Assessing Needs, Perceptions, and Curricular Gaps

Authors:
Shazia Naseem, MD; Affaf Gul, MD; Renee M. Moadel, MD; Syed Mahmood, MD
Division of Nuclear Medicine, Department of Radiology
Montefiore Medical Center, The University Hospital for Albert Einstein College of Medicine
Bronx, NY 10461
Emails: snaseem@montefiore.org; agul@montefiore.org; rmoadel@montefiore.org; syemahmood@montefiore.org

Background:
Artificial Intelligence (AI) in medical imaging, particularly in nuclear medicine, is rapidly transforming diagnostic workflows (e.g., automated segmentation, image quality enhancement, noise reduction) and decision-making processes (e.g., diagnosis, prognosis, and theranostics). For example, AI has been applied in tumor segmentation in PET imaging, lesion detection and tracking in PSMA PET scans, and automated quantification of amyloid and tau burden in neuroimaging. AI-driven tools are also being used to enhance SPECT and PET image reconstruction, enabling faster acquisition times and lower radiotracer doses without compromising diagnostic quality. Furthermore, deep learning algorithms are being developed to predict treatment response from baseline PET scans, assist in radiomics feature extraction, and stratify risk in oncology and cardiology using multi-parametric imaging data. AI applications in workflow optimization, such as automated triage, report generation, and scheduling based on predicted case complexity, are also gaining traction in nuclear medicine departments.

Despite its growing adoption, there is limited literature on educating nuclear medicine professionals about AI's capabilities, limitations, and clinical applications. As the field evolves, there is an urgent need to equip physicians, trainees, and technologists with the knowledge and skills to critically assess and effectively utilize AI tools in clinical practice.

Objective:
This study aims to understand the awareness of AI, the perceived need for AI training, current knowledge gaps, utility, requirements of an artificial intelligence curriculum, and barriers to implementing AI training in Nuclear Medicine. The ultimate goal is to inform the development of a comprehensive curriculum that enhances knowledge, practical skills, and confidence in applying AI in nuclear medicine imaging.

Methods:
Following IRB exemption, an anonymous Likert scale-based survey was developed in collaboration with experts in nuclear medicine, radiology, and medical imaging informatics.

The survey was distributed via email to attendings, residents, and fellows in the Division of Nuclear Medicine at Montefiore Medical Center. The questionnaire assessed participants' familiarity with AI concepts, understanding of AI applications specific to nuclear imaging, perceived impact on clinical practice, and interest in a formal structured AI education.

Results:
All 13 participants completed the survey; of which there were 7 attendings and 6 trainees.

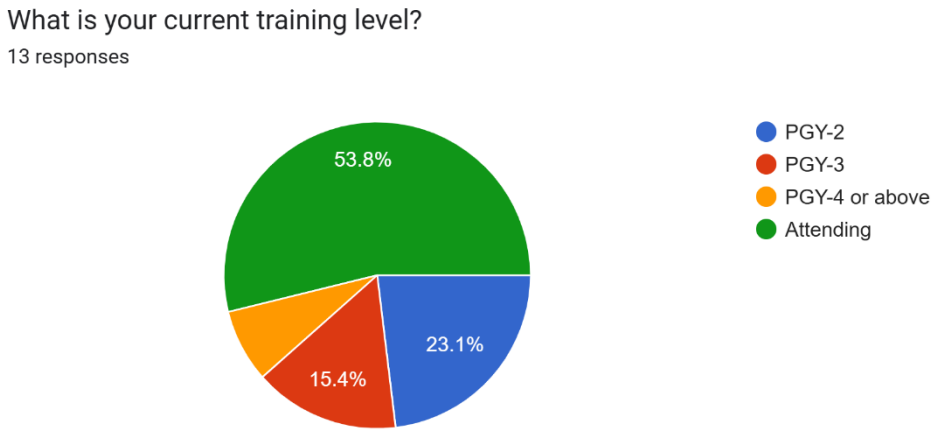

Forty-two percent (42%) of participants strongly agreed, and an additional 8% agreed that they were aware of AI applications in nuclear medicine.

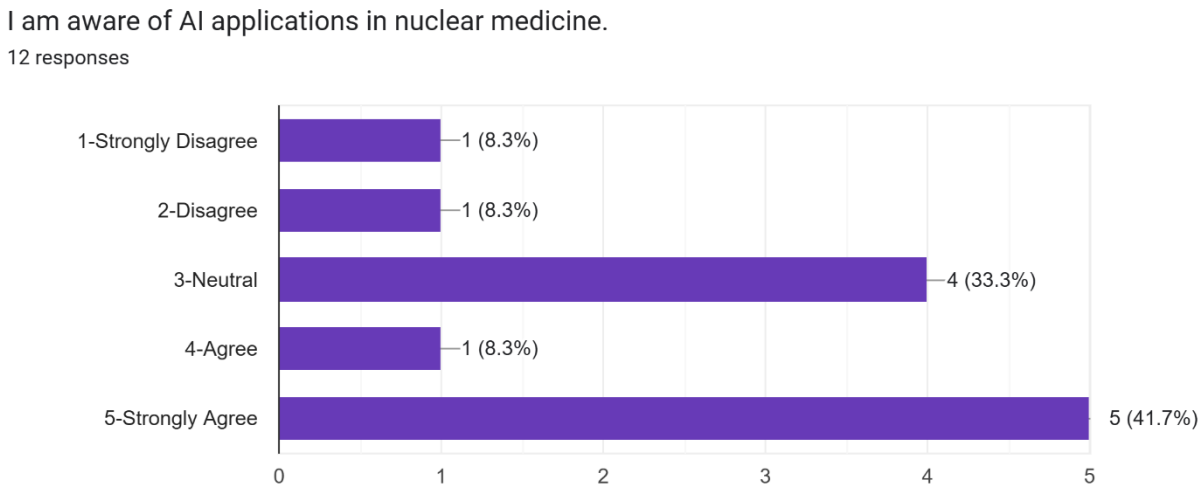

The majority (54%) of participants strongly agreed, and an additional 31% agreed that they were interested in learning more about AI applications in nuclear medicine.

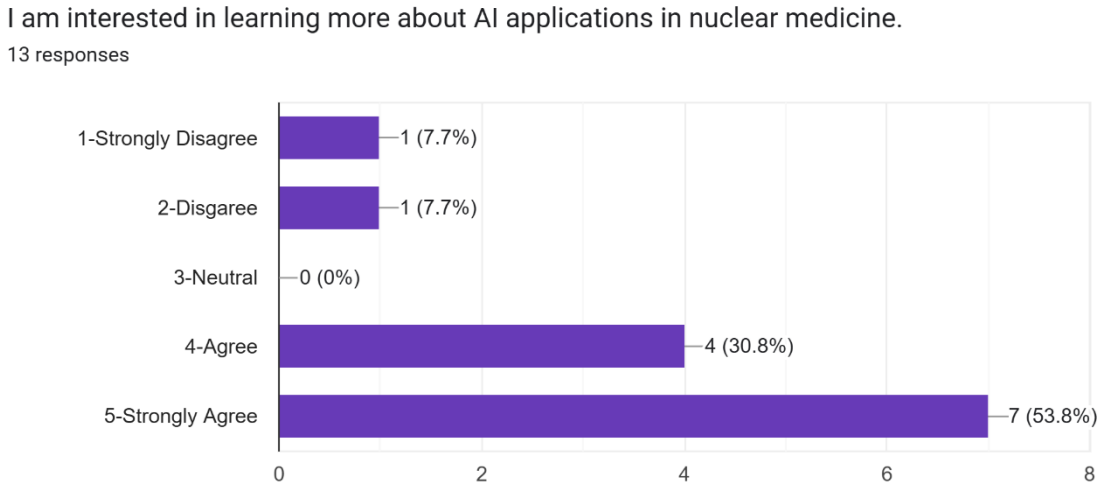

The majority (50% agreed and 25% strongly agreed) agreed that there is a lack of structured AI education or curriculum in our training program.

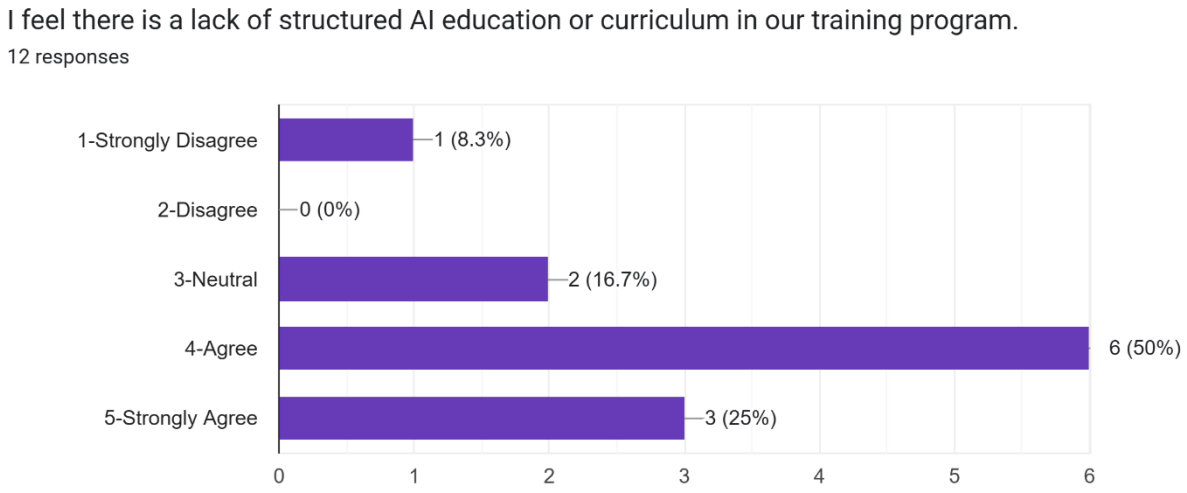

The majority (54% agreed and 39% strongly agreed) agreed that a hands-on approach is a better way of learning when compared to observation.

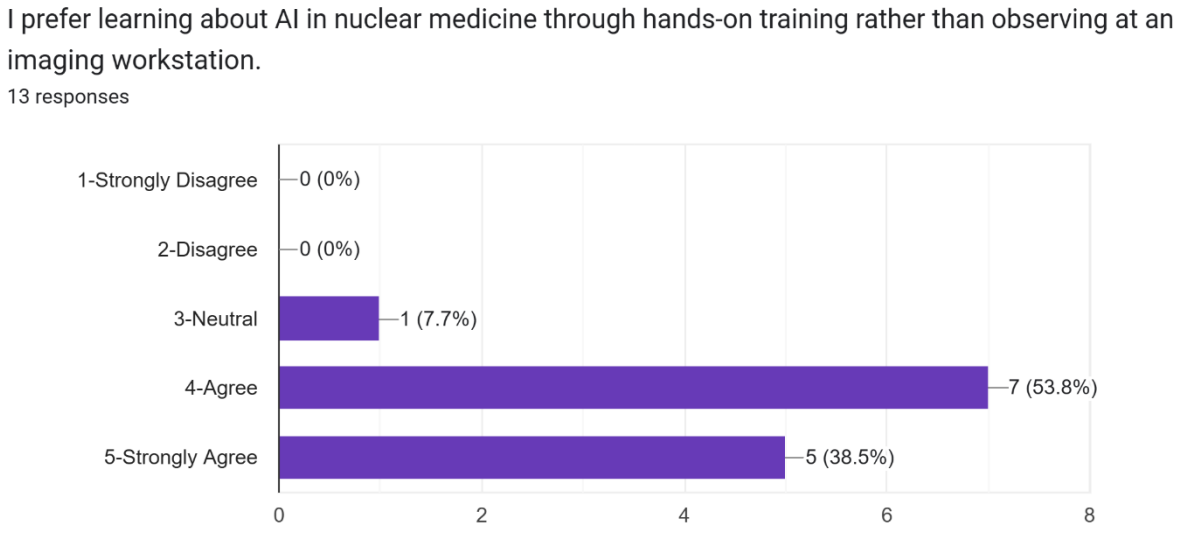

Conclusion:

This study provides vital information about nuclear medicine attendings, residents and fellows' perspectives on the awareness, perceptions, current knowledge, utility, educational needs, and barriers to implementing AI applications in nuclear medicine. We revealed that about half of our nuclear medicine attendings and trainees were aware of, and most would like to learn about AI applications in nuclear medicine. The preferred educational format was hands-on training. Foreseen barriers included the absence of a formal curriculum, limited institutional support, and restricted access to relevant tools or mentorship.

References:

1. Saboury B, Bradshaw T, Boellaard R, et al. Artificial Intelligence in Nuclear Medicine: Opportunities, Challenges, and Responsibilities Toward a Trustworthy Ecosystem. *J Nucl Med.* 2023;64(2):188-196. doi:10.2967/jnumed.121.263703
2. Seifert R, Weber M, Kocakavuk E, Rischpler C, Kersting D. Artificial Intelligence and Machine Learning in Nuclear Medicine: Future Perspectives. *Semin Nucl Med*. 2021;51(2):170-177. doi:10.1053/j.semnuclmed.2020.08.003
3. Currie GM, Hawk KE, Rohren EM. The potential role of artificial intelligence in sustainability of nuclear medicine. *Radiography (Lond)*. 2024;30 Suppl 1:119-124. doi:10.1016/j.radi.2024.03.005

4. Lopes L, Lopez-Montes A, Chen Y, et al. The Evolution of Artificial Intelligence in Nuclear Medicine. *Semin Nucl Med*. 2025;55(3):313-327. doi:10.1053/j.semnuclmed.2025.01.006
5. Visvikis D, Lambin P, Beuschau Mauridsen K, et al. Application of artificial intelligence in nuclear medicine and molecular imaging: a review of current status and future perspectives for clinical translation. *Eur J Nucl Med Mol Imaging*. 2022;49(13):4452-4463. doi:10.1007/s00259-022-05891-w
6. Gheisari F, Ebrahimi N, Vali R. Artificial Intelligence in Nuclear Medicine: Current Applications and Future Prospects. *American Journal of Biomedical Science & Research*. 2024;21(5). doi:10.34297/AJBSR.2024.21.002879.

POSTER #20

Abstract

Title:
Development and Validation of the Nonuniform Intense Bowel Uptake (NIBU) Score: A Standardized Semi-Quantitative Tool for Assessing FDG Intense Bowel Uptake Heterogeneity on PET/CT

Authors:
Eduardo A. Sanchez-Perez, MD; Syed Mahmood, MD; Ana Valdivia, MD
Division of Nuclear Medicine, Department of Radiology
Montefiore Medical Center, The University Hospital for Albert Einstein College of Medicine
Bronx, NY 10461
E-mails: esanchezpe@montefiore.org, syemahmood@montefiore.org, avaldivi@montefiore.org

Background:
Physiologic F-18 fluorodeoxyglucose (FDG) uptake in the bowel is a frequent finding on routine oncologic PET/CT, often manifesting as uneven or diffusely increased activity that can obscure mesenteric or nodal evaluation. Unlike the myocardium, where well-established pre-scan preparation protocols (e.g., dietary manipulation, insulin/glucose loading) reliably modulate FDG uptake, no methods exist to modulate physiologic bowel activity. Moreso, no standardized method exists to describe physiologic bowel activity. Variability in bowel activity is influenced by motility, diet, medications (e.g., metformin), gut microbiota, and its leaky capillary endothelium. To address this variability, we propose a semi-quantitative tool termed the Nonuniform Intense Bowel Uptake (NIBU) score to classify the degree of physiologic bowel FDG uptake heterogeneity and intensity observed on PET/CT.

Methods:
A retrospective review was performed of adult patients (>18 years) who underwent standard whole-body FDG PET/CT (base of skull to mid thighs) between January 2 and January 19, 2024, at Montefiore Medical Center. Exclusion criteria included: abnormal radiotracer biodistribution, bowel malignancy, prior anastomosis, or active abdominopelvic neoplasm precluding bowel assessment. Of 77 patients, 67 met inclusion criteria. We present our findings from a pilot study of the NIBU score applied to six representative cases.

Figure 1. NIBU scoring system for the different bowel segments and uptake patterns: **Increased Bowel Uptake** is defined as any segment with an SUV 0.5 units greater than the **Liver SUV mean**.

Bowel Segment	Relative volume of segment compared with rest of bowel (burden) + adjacent Viscera/reticulo-endothelial Tissue Density	Score
Stomach	Medium-large volume burden and mild-moderate surrounding density.	2 point
Duodenum	Small volume burden and high surrounding density	1 point
Ileum/jejunum	Large volume burden and minimal surrounding density	2 point
Ascending Colon	Medium volume burden and minimal surrounding density.	1 point
Transverse Colon	Medium volume burden and minimal surrounding density.	1 point
Descending Colon	Medium volume burden and minimal surrounding density.	1 point
Rectosigmoid	Medium volume burden and high surrounding density	2 points

Uptake Patterns (Score Modifiers)

Uptake Pattern	Definition	Score
Extensive	(1) Extensive FDG activity involving 100% of the segment.	1.0
Segmental Diffuse	(1) Diffuse continuous activity confined to a segment that does not involve 100% of the segment. (2) (2) Pattern does not meet segmental patchy definition.	0.7
Segmental Patchy	(1) Diffuse non-continuous/patchy activity across the segment that if meshed would not involve more than 50% of the segment. (2) Increased continuous uptake that measures > 2.5cm (3) In the ileum/jejunum, multifocal activity with at least 5 foci.	0.5
Confluent Regional	(1) Focal uptake that is not round and does not measure greater than 2.5cm. (2) Ileum/jejunum, multifocal (<5 foci).	0.2
Isolated Round Focus	(1) Isolated, round activity	0.1

Results:
Patients (n=67) had a mean age of 65.1 years (males = 25, females = 43). The most common indications were lung cancer (32%), and hematopoietic malignancy (24%) in males, and hematopoietic malignancy (33%) and breast cancer (21%) in females.
Liver SUV mean ranged from 1.4 – 3.4 (mean 2.38 +/- 0.68). Total NIBU scores ranged from 1.3 - 7.0 (mean 3.6 +/- 1.9), corresponding to mild-to-moderate intense uptake heterogeneity. Two cases demonstrated mild activity (NIBU =1-2), three showed mild-to-moderate heterogeneity (NIBU = 3 - 4), and one exhibited moderate-to-high heterogeneity (NIBU = 7). Higher scores correlated with extensive or segmental activity involving multiple bowel segments, whereas lower scores reflected localized, confluent, or patchy uptake limited to a few anatomic segments. Interobserver agreement and validation are planned.

Example cases (figure 2) illustrate mild (NIBU = 1) and moderate-to-high (NIBU = 7) uptake patterns.

Conclusion:
This pilot application of the NIBU scoring tool demonstrates feasibility in characterizing physiologic bowel FDG uptake heterogeneity and intensity on FDG PET/CT. The semi-quantitative framework provides a structured approach for describing nonuniform increased bowel activity, potentially facilitating reproducibility across readers and studies. Although limited by small sample size and lack of interobserver validation, future work will expand the cohort, test reliability, refine weighting schemes, and evaluate the tool in a prospective clinical trial that will test whether a 6-day MiraLAX regimen, a 24-hour low-carbohydrate low-residue diet, and a single dose of dicyclomine given by injection can reduce FDG-intense bowel uptake heterogeneity (NIBU score).

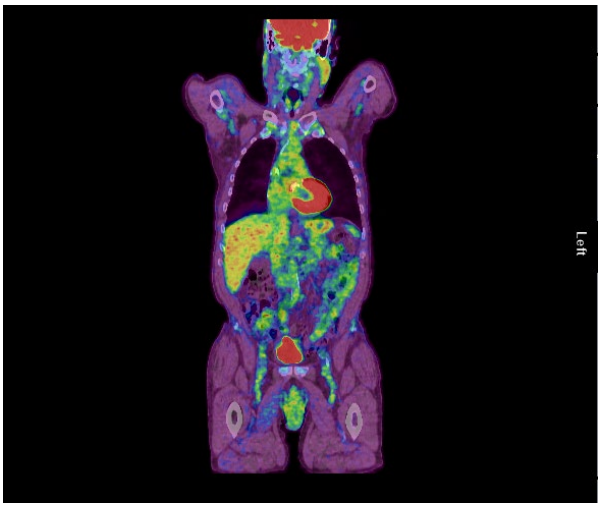

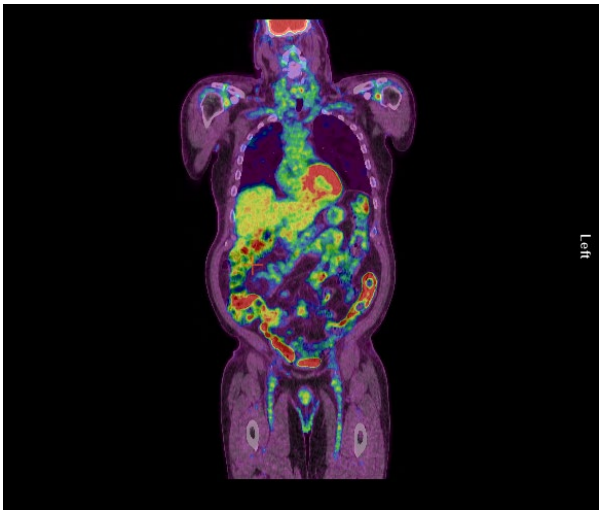

Figure 2. Coronal fused FDG PET/CTs of patients with mild (NIBU=1, top image) and moderate-to-high (NIBU=7, bottom image) degree of FDG-intense bowel uptake heterogeneity.

POSTER #21

FDG PET/CT Lights the Way: When Conventional Imaging Falters in Suspected Infection and Inflammation

Muhammad Awais Ashraf, D.O.
Radiology Resident, R4
muhammad.a.ashraf90@gmail.com
Hartford Hospital

Veronica Periera, M.D.
Radiology Resident, R3
vmp823@gmail.com
Hartford Hospital

Racquel Helsing, M.D.
Radiology Resident, R4
racquelhelsing@gmail.com
University of Connecticut

Prasanta Karak, M.D.
Attending Physician
Prasanta.Karak@hhchealth.org
Hartford Hospital, Jefferson Radiology

Background

^{18}F-Fluorodeoxyglucose positron emission tomography/computed tomography (^{18}F-FDG PET/CT) serves as a conclusive imaging technique for identifying infectious and inflammatory processes when conventional anatomic imaging yields equivocal results. This method is based on the enhanced glycolytic activity of activated inflammatory cells, specifically neutrophils, macrophages, and lymphocytes. The increased metabolism results in the preferential accumulation of a glucose analogue at the sites of infection. Functional-anatomic imaging technique integrates metabolic localization with structural context. It enhances the detection sensitivity for hidden disease foci, delineates the extent of the disease, and supports targeted interventions. This approach is particularly valuable for hardware-associated and multifocal infections where standard diagnostic methods are limited by restricted field of view, vague symptoms, and/or inconclusive results.

Purpose

The objective is to systematically demonstrate how FDG PET/CT resolves diagnostic challenges in complex infectious diseases. This includes highlighting typical uptake patterns, providing comprehensive disease mapping, and illustrating the impact on patient clinical management.

Methods

Nine representative cases referred following nondiagnostic conventional imaging underwent whole-body FDG PET/CT using standardized protocols. Radiotracer uptake patterns and corresponding CT anatomy were interpreted and clinically validated using available operative/endoscopic findings, microbiological data, and supplementary imaging. Cases were categorized as vascular prosthetic graft infection, musculoskeletal infection, polyarticular septic arthritis with pyomyositis, and fever of unknown origin.

Results and Cases

Vascular Prosthetic Graft Infection (Cases 1–4):

Case 1: A patient with Takayasu arteritis with aorto-bifemoral graft extending from the descending aorta along the left lateral abdominal wall to a bifemoral graft in the midline, which then connected to the femoral arteries in the superficial pelvis. PET/CT imaging revealed intense perigraft hypermetabolism, soft-tissue nodularity, and fluid collections

associated with the graft, indicating a probable graft infection. Cultures from diagnostic drainage grew *Cutibacterium* and *Kocuria*, organisms not typically highly virulent. Given the thoraco-bifemoral bypass graft and the subsequent inline reconstruction, a surgical approach would be an extremely challenging procedure associated with a very high risk of perioperative morbidity and mortality. Consequently, the patient will require life-long suppressive antibiotics with active surveillance.

Case 2: Aortobifemoral graft with endoscopically confirmed aortoenteric fistula exhibited patchy linear perigraft hypermetabolism with bilateral inguinal extension.

Case 3: Aortic arch graft showed circumferential peri-arch hypermetabolism, distinguishing active infection from sterile endoleak.

Case 4: Right iliofemoral graft demonstrated focal metabolic activity with concurrent inflammatory changes surrounding abdominal mycotic aortic aneurysm.

Musculoskeletal Infection (Cases 5–7):

Case 5: Vertebral osteomyelitis/spondylodiscitis manifested as marked L3-L4 hypermetabolism with osteolytic lesions, endplate erosions, and paraspinal/epidural extension.

Case 6: Diabetic foot demonstrated contiguous osteomyelitis of fifth metatarsal with inseparable soft-tissue hypermetabolism extending from ulcer bed into osseous structures.

Case 7: Charcot neuroarthropathy showed radiotracer uptake in the soft tissues next to the ulcer and in the articular structures of the midfoot. Importantly, there was no distinct osseous avidity, which helped prevent the overcalling of osteomyelitis, even when nonspecific marrow abnormalities were present on MRI.

Polyarticular Septic Arthritis with Pyomyositis (Case 8): Whole-body PET/CT showed identified multifocal infection. It revealed avid synovitis in the glenohumeral and sternoclavicular joints, with extension into the rotator-cuff and pectoralis muscles, with intramuscular abscesses. Additional infected foci were found in the wrist, hip/iliopsoas region, pubic symphysis, and midfoot, several with small collections.

Fever of Unknown Origin (Case 9): PET/CT showed a rim-pattern hypermetabolic abscess in the left chest wall. Furthermore, it identified occult soft-tissue foci near the proximal femur and sacrum, extending into the greater sciatic foramen, identified only on the retrospective review of the initial CT. This information was critical in guiding subsequent drainage procedures and optimizing antimicrobial treatment.

Conclusion

FDG PET/CT is a valuable diagnostic tool for identifying infection and inflammation when conventional imaging proves inconclusive. Principal advantages include reliable differentiation of infection from metabolically inactive mimics, comprehensive disease extent delineation encompassing perigraft tracts, and systematic multifocal disease detection. PET/CT integrates whole-body functional and anatomic imaging data, often assisting in resolving diagnostic uncertainty and delineating disease extension. This leads to site-specific, actionable care, ultimately optimizing therapeutic targeting and improving patient outcomes.

POSTER #22

Optimization of a Numerical Observer for Use in Pediatric Reconstructive Pediatric SPECT Kidney Images

Authors: Sarah Van Hoesen (Worcester Polytechnic Institute), Dr. Ted Treves (Harvard Medical School), Dr. Michael King (UMass Chan Medical School), Dr. William McCarthy (Worcester Polytechnic Institute)

Background

It is imperative that doctors have access to high quality, accurate diagnostic images. One opportunity to improve image quality in the reconstructed image takes place after the initial image acquisition. During this reconstruction, many methods can be employed to improve the image quality such as motion correction, de-noising, and attenuation correction. The ultimate goal of improving image quality is to improve patient outcomes through diagnostic accuracy or reduced radiation dose. DMSA-Tc99m SPECT is often used to diagnose pyelonephritis which when left untreated can result in kidney failure. Early lesions can be small and hard to detect so slight changes in image quality can have great effect. Therefore, the reconstruction processes must be assessed relative to clinical significance. The gold standard for this assessment is a physician observer localization receiver operating characteristic (LROC) study, but these are both expensive and time consuming. We have created a numerical observer (NO) that mimics the performance of experts in order to pre-optimize our reconstruction prior to carrying out a physician observer study.

Methods

We developed a non pre-whitening NO to detect lesions in pediatric DMSA renal scans. We are optimizing the NO to match performance data we are obtaining from a pilot expert observer study of 220 total simulated scans of XCAT phantoms, 147 with uniquely inserted lesions. These images were presented to four expert observers in a forced choice LROC study to identify lesions in the outer cortex. Though the observer study is ongoing, we plan to vary the NO's input parameters until its performance closely matches the expert observer LROC curves in both shape and area under the curve.

Our numerical observer gives each point on the outer surface of the kidney image a score that corresponds to the likelihood that point is within a lesion. This score is calculated by summing over the pixels of a difference map of the study image and the noise-free, lesion-free image weighted by a lesion template. The point with the highest likelihood value is the numerical observer's localization and we convert the score into the confidence values used in LROC analysis. The NO generates the lesion template by

using a cylinder oriented normal to the surface to take a cutout of the kidney at the given point.

Results

We have early results from our expert observers and are running preliminary tests of our NO's ability to be tuned. Results indicate that the general shape of the LROC curve and area under that curve can be matched with that of the expert observers. We expect that this accuracy will increase as we incorporate more data.

Conclusion

After collection of the expert observer data is completed, we will finalize the tuning of the NO to that data. Given that the results are as expected, we will be able to use this optimized NO to rapidly test advanced reconstruction and post processing techniques we are developing and optimize their parameters prior to further expert observer studies.

POSTER #23

Signs in Brain Death Scintigraphy: the Good, the Bad and the Useless.

Lionel S. Zuckier. Department of Radiology, Division of Nuclear Medicine, Columbia University Medical Center, New York, NY

Background: There has been significant recent activity in the clinical and imaging arenas related to death by neurologic criteria (DNC) including new clinical and SNMMI/EANMMI guidelines; this is therefore a good juncture to survey scintigraphy for DNC. We have reviewed the value of various "signs" that have appeared in the imaging literature.

Methods: Literature related to DNC and scintigraphy was reviewed and the presence of "signs" and their implication was recorded.

Results: Four nuclear medicine signs of variable usefulness were identified and are clarified in this presentation.

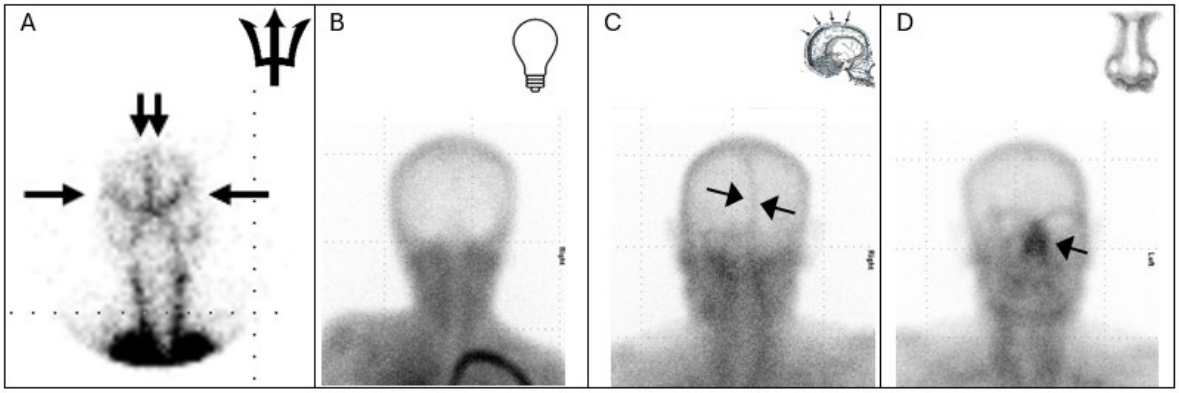

A - Trident Sign: On flow phase, checking for perfusion in the anterior and middle cerebral arteries is a **mandatory** component of all DNC perfusion (hydrophilic and lipophilic) studies. Activity in any part of the trident indicates presence of blood flow.

B - Empty Lightbulb Sign: On parenchymal phase, checking for activity localizing within the calvarium is a **mandatory** component of all DNC lipophilic studies. Activity in any part of the cranium ("lightbulb") indicates presence of perfusion.

C - Sagittal Sinus Sign: On blood pool phase, presence of activity within the superior sagittal sinus, once considered to be a soft-sign of intracranial blood flow, is now considered **non-contributory**, as activity may come from collateral scalp vessels.

D - Hot Nose Sign: On blood pool and parenchymal phase, presence of a "hot" nose has been touted as a sign of DNC due to increased flow to the face in presence of absent brain flow. In fact, this finding is **non-specific** for DNC and can therefore be **misleading**. Why look at the nose instead of at the brain?

Conclusions: Signs in imaging are a memorable and concise way of conveying critical imaging features however like any diagnostic measure, they must be critically assessed. Useless or potentially misleading signs may misdirect inexperienced readers and cause harm. In scintigraphic perfusion studies performed in the context of DNC, the "trident" and "empty light bulb" signs are reliable and in fact mandatory. The "hot nose" sign is misleading and should not be used, whilst the "sagittal sinus" sign is simply non-contributory.

POSTER #24

Primary Hepatocellular Carcinoma Incidentally Detected on PSMA PET/CT

Kush Patel, MD[1], William Y. Raynor, MD[1], Samar Hajj, MD[1], Anupriya Barot, MD[1], Don Goldstein, MD[1], Rizvan Azimzade, MD[2], Stephen Sozio, DO[1], Jeffrey S. Kempf, MD, FACR[1]

1. Department of Radiology, Rutgers Health, Robert Wood Johnson Medical School, New Brunswick, NJ, USA.
2. Department of Medicine, Rutgers Health, Robert Wood Johnson Medical School, New Brunswick, NJ, USA.

Background: Prostate-specific membrane antigen (PSMA) PET/CT has emerged as a valuable imaging modality for the detection and staging of prostate cancer. PSMA ligands labeled with ^{68}Ga or ^{18}F are used for diagnostic PET imaging, while ^{177}Lu- and ^{225}Ac-labeled agents can be used for targeted radiotherapy [1]. Although PSMA expression is often associated with prostate cancer, high levels of PSMA uptake have been documented in several non-prostatic malignancies, including salivary gland tumors, thyroid cancer, renal cell carcinoma, glioblastoma, breast cancer, and lung cancer [2]. PSMA expression has also been observed in hepatocellular carcinoma (HCC), suggesting a potential role for PSMA PET/CT in the detection and characterization of primary liver malignancies. We present a case of PSMA-avid HCC incidentally detected on PSMA PET/CT performed for evaluation of recurrent prostate cancer in a patient with chronic hepatitis C.

Methods: A 72-year-old male with a history of chronic hepatitis C, prostate adenocarcinoma status post definitive radiation therapy with 15 Gy in 5 fractions one year prior with unknown PSA nadir, and end-stage renal disease on dialysis underwent PSMA PET/CT for evaluation of biochemical recurrence of prostate cancer, with a PSA level of 5.8 ng/mL at the time of imaging. PSMA PET/CT revealed heterogeneous nonspecific uptake within the prostate gland. Notably, there was intense uptake (SUVmax 14.9) in a solid exophytic hepatic mass measuring 5.3 cm in segment 5. Laboratory studies at that time were notable for an elevated alpha-fetoprotein (AFP) of 14,826 ng/mL and mildly elevated AST and ALT levels (54 and 58 U/L, respectively). The tumor was staged cT1bN0, and the patient subsequently underwent SBRT of 67.5 Gy in 15 fractions directed at the hepatic lesion; there was no interval prostate cancer directed therapy.

Results: Follow-up PSMA PET/CT performed 5 months later for follow-up of prostate cancer due to persistent elevation of PSA to 3.4 demonstrated interval decrease in the size of the liver lesion to 2.4 cm with no residual PSMA uptake. This correlated with the clinical response to therapy. Histopathologic confirmation of primary HCC was not obtained because the patient met LI-RADS LR-5 criteria, and the elevated AFP combined with response to locoregional therapy further supporting diagnosis. Although PSMA PET/CT is widely used for prostate cancer, PSMA expression has been reported in primary HCC [3-5], with recent studies demonstrating high sensitivity for lesion detection. In a prospective study by Shamim et al., 38 of 41 patients with known HCC demonstrated PSMA uptake on PSMA PET/CT [6]. Similarly, Kesler et al. reported PSMA uptake in 36 of 37 HCC lesions, with PSMA PET/CT outperforming FDG PET/CT in overall lesion detection [7].

Conclusions: This case highlights the potential for a future role of PSMA PET/CT in the detection of HCC. Incidental hepatic PSMA uptake should not be presumed to be metastatic prostate cancer, especially in high-risk patients. PSMA PET/CT may have a role in HCC imaging, especially in assessing response to locoregional therapy as in this case.

References

1. Georgakopoulos, A., A. Bamias, and S. Chatziioannou, *Current role of PSMA-PET imaging in the clinical management of prostate cancer.* Ther Adv Med Oncol, 2023. **15**: p. 17588359231208960.
2. Lauri, C., et al., *PSMA Expression in Solid Tumors beyond the Prostate Gland: Ready for Theranostic Applications?* J Clin Med, 2022. **11**(21).
3. Huang, H.L., T.J. Zhen Loh, and P.K. Hoe Chow, *A Case of Well-differentiated Hepatocellular Carcinoma Identified on Gallium-68 Prostate-specific Membrane Antigen Positron Emission Tomography/Computed Tomography.* World J Nucl Med, 2018. **17**(2): p. 102–105.
4. Das, J., et al., *Prostate-specific Membrane Antigen-expressing Hepatic Lesion: Metastatic or Hepatocellular Carcinoma.* Indian J Nucl Med, 2020. **35**(1): p. 58–60.
5. Sasikumar, A., et al., *68Ga-PSMA PET/CT imaging in primary hepatocellular carcinoma.* European journal of nuclear medicine and molecular imaging, 2016. **43**(4): p. 795–796.
6. Shamim, S.A., et al., *A prospective study of (68)Ga-PSMA PET/CT imaging of HCC as diagnosed on conventional imaging to evaluate for potential (177)Lu-PSMA therapy.* Ann Nucl Med, 2024. **38**(2): p. 103–111.
7. Kesler, M., et al., *(68)Ga-PSMA is a novel PET-CT tracer for imaging of hepatocellular carcinoma: A prospective pilot study.* J Nucl Med, 2019. **60**(2): p. 185–191.

POSTER #25

Title: Added Value of Brain [68Ga]-DOTATATE PET/CT and PET/MRI in Assessing Internal Auditory Canal Involvement in Skull Base Meningioma.

Authors: Preeti Kakkar, Valentina Marulanda Corzo, Kellen Vo Vu, Rajiv S. Magge, Andrew Brandmaier , Joseph R. Osborne, Jana Ivanidze.

Introduction

Meningiomas are the most common extra-axial brain tumors and frequently express somatostatin receptor subtype 2 (SSTR2), making them highly amenable to imaging with [68Ga]-DOTATATE PET/CT or PET/MRI. While MRI remains the gold standard for meningioma evaluation, DOTATATE PET can provide complementary information regarding tumor extent, particularly for skull base lesions. Cerebellopontine angle (CPA) meningiomas typically form a broad-based dural attachment at the CPA-internal auditory canal (IAC) junction without invading the IAC, in contrast to CPA schwannomas which commonly extend into the IAC. However, CPA meningiomas may occlude the IAC, causing inflammatory dural thickening and enhancement that can mimic IAC invasion by tumor on MRI. Our purpose was to illustrate the added value of DOTATATE PET in this clinical context.

Methods

Patients were identified from our prospectively enrolled, IRB approved institutional registry of approximately 350 individuals with known or suspected meningioma or other SSTR2-positive brain or skull base tumors who underwent [68Ga]-DOTATATE PET/CT or PET/MRI as part of clinical care, performed according to our previously published institutional protocol), who had tumors with characteristic MRI features of CPA meningioma (dural based, enhancing mass at the cerebellopontine angle), as well as MRI demonstrating contiguous extension of contrast enhancement into the IAC (CE-IAC). Surgical and radiation therapy (RT) history, clinical and demographic characteristics, and subsequent management post PET were reviewed for all patients. Qualitative assessment of extent of [68Ga]-DOTATATE avidity was performed by a dual board certified neuroradiologist and nuclear medicine physician, evaluating for extension of enhancement and DOTATATE avidity into the IAC. Quantitative assessment was performed evaluating maximum SUV (SUVmax) and SUV ratio referencing the superior sagittal sinus (SUVRsss) of each CPA tumor and separately, SUVmax of each contiguous CE-IAC. Statistical analyses included descriptive statistics and paired non-parametric t

test (Wilkoxon matched-pairs signed rank test) to assess differences between [68Ga]-DOTATATE PET SUVmax of CPA tumors and their corresponding CE-IAC.

Results

Seventeen patients met inclusion criteria (15/17 (88%) women; WHO grade 1/2/unknown: 9/2/6; mean age 68 years (range, 42-85); 11/17 (65%) had prior surgery; 15/17 (88%) had prior radiotherapy).

Mean (95% confidence interval (CI)) SUVmax was 34.2 (22.6-45.85) for the CPA tumors, and 3.3 (1.6-4.9) for the corresponding CE-IAC lesions (p-value: <0.0001). Mean (95% CI) SUVRsss was 24.2 (16.4-32.0) for CPA tumors, and 2.3 (1.3-3.3) for the corresponding CE-IAC lesions (p-value: <0.0001). Statistical analysis results along with an illustrative patient example are summarized in **Figure 1**.

Discussion

[68Ga]-DOTATATE PET has demonstrated excellent clinical utility in delineating meningiomas, particularly in the postsurgical and post-radiotherapy setting. Here, we show the utility of [68Ga]-DOTATATE PET in the specific context of CPA meningiomas. CE-IAC demonstrated low SUVmax and SUVRsss (below published diagnostic threshold for meningiomas), confirming that meningiomas do not invade the IAC. Our findings underscore the utility of tumor delineation in this patient population, allowing an optimized treatment approach in this anatomically complex location.

Conclusion

[68Ga]-DOTATATE PET is a valuable adjunct to MRI in evaluating CPA meningiomas, improving diagnostic confidence and enabling more precise surgical and radiotherapy planning.

Keywords:[68Ga]-DOTATATE, PET/CT, PET/MRI, meningioma, skull base, internal auditory canal

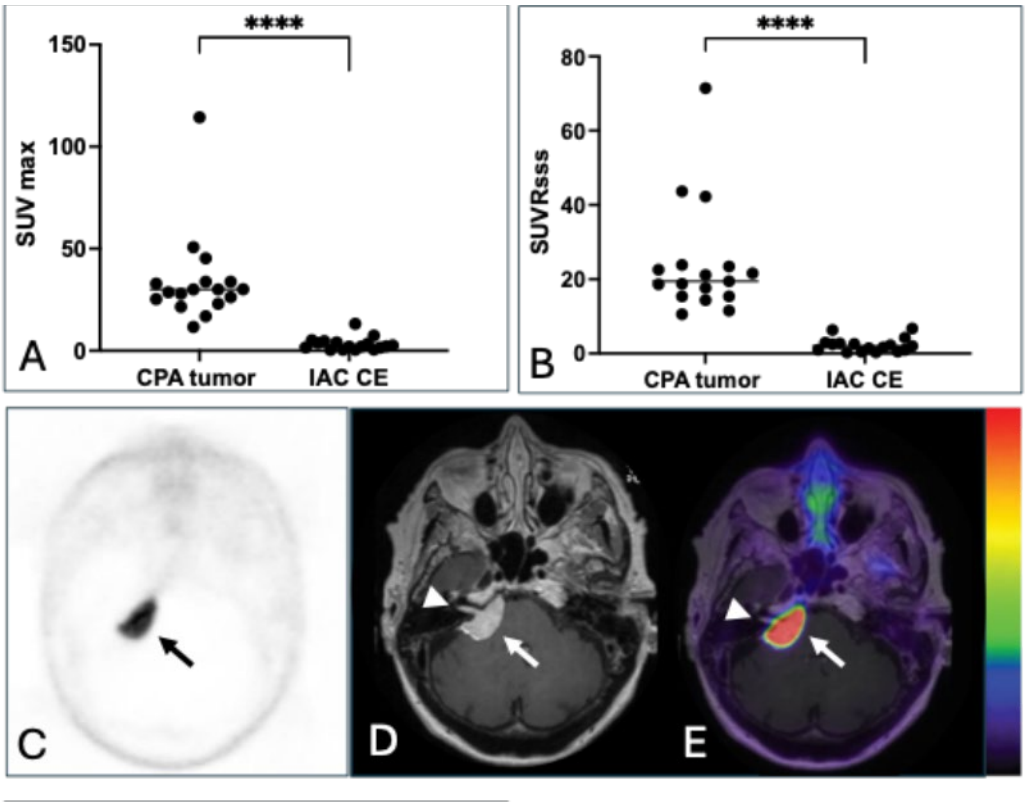

Figure 1 [68Ga]-DOTATATE PET/MRI-based evaluation of cerebellopontine angle (CPA) meningiomas and contiguous enhancement within the internal auditory canal (IAC CE). (A) Scatter plot demonstrating marked difference in SUVmax between CPA meningiomas and IAC CE. **(B)** Scatter plot demonstrating marked difference in SUV ratio referencing superior sagittal sinus (SUVRsss) between CPA meningiomas and IAC CE. **** indicates p-value<0.0001 resulting from a paired non-parametric t-test comparing SUVmax and SUVRsss between CPA tumors and corresponding IAC CE lesions. **(C - E)** Representative patient example. Axial [68Ga]-DOTATATE PET demonstrates intense circumscribed avidity in the right CPA (arrow), corresponding to avidly enhancing dural-based mass on post-gadolinium T1-weighted axial MRI (arrow in D and E). MRI additionally demonstrates contiguous extension of avid enhancement into the IAC (arrowhead in D), which is non-DOTATATE avid (arrowhead in E).

References:

Ivanidze J, Chang SJ, Haghdel A, et al. [Ga68] DOTATATE PET/MRI-guided radiosurgical treatment planning and response assessment in meningiomas. Neuro-Oncology. Published online March 29, 2024. doi:10.1093/neuonc/noae067

Ivanidze J, Roytman M, Lin E, et al. Gallium-68 DOTATATE PET in the Evaluation of Intracranial Meningiomas. J Neuroimaging. 2019;29(5):650-656. doi:10.1111/jon.12632

Perlow HK, Nalin AP, Handley D, et al. A Prospective Registry Study of 68Ga-DOTATATE PET/CT Incorporation Into Treatment Planning of Intracranial Meningiomas. Int J Radiat Oncol Biol Phys. 2024;118(4):979-985. doi:10.1016/j.ijrobp.2023.10.014

Rachinger W et al. Positron emission tomography with ^68Ga-DOTATATE for differentiation of tumor and scar tissue in meningiomas. Eur J Nucl Med Mol Imaging. 2015;42(3):419–427.

POSTER #26

Title: PSMA PET/CT Studies at Time of Suspected Recurrence of Prostate Cancer in Patients Post Radical Prostatectomy

Authors: Jaun Young-Johnson[3] , BA, Yi Li [1,2] , MD, Simin Dadparvar [1] , MD;

Division of Nuclear Medicine and Molecular Imaging, Department of Radiology, Temple University Hospital [1] , Fox Chase Cancer Center [2] and Lewis Katz School of Medicine at Temple University [3] , Philadelphia, PA 19140

Background: Prostate cancer is the second most frequently diagnosed cancer and a frequent cause of cancer-death among men worldwide. For patients with intermediate- to high-risk prostate cancer, radical prostatectomy is often the standard definitive treatment. However, despite such interventions, a notable portion of patients experience biochemical recurrence, as indicated by a rise in post-surgical PSA levels. This is largely due to limitations in conventional imaging modalities – such as computed tomography (CT) and magnetic resonance imaging (MRI) – which fail to detect locoregional and distal metastasis at time of local recurrence.

The purpose of this study is to perform a retrospective chart review to investigate the detection of malignancy in recurrence of prostate cancer in patients previously treated with radical prostatectomy.

Method: We retrospectively reviewed 60 PSMA PET/CT studies in 34 patients with suspicion for recurrent prostate cancer (age range 46-77, mean age 65.2 years, median age 66) between March 28, 2022- June 24, 2024, with suspicion for metastasis (showed evidence of biochemical recurrence) and had known metastasis who underwent PSMA PET/CT scans post prostatectomy. The patients' initial PSA and Gleason scores were reviewed. Patients' response to radiation with PSA was measured. Following recurrence with elevation of PSA level the PET/CT study was performed after intravenous administration of a PSMA PET imaging agent (Pylarify, LOCAMETZ, ILLUCCIX or Posiluma).

Results: The median PSA level at initial diagnosis was 6.9 ng/ml (range, 3 to 29), while the median PSA level at the time of PSMA PET/CT was 1.63 ng/ml (range, 0.06 to 600). The median Gleason score among patients was 7 (range 6(3+3) to 10(5+5). Notably, 46 of 60 (76.7%) studies showed evidence of local recurrence, regional metastasis, or distant metastasis.

Conclusion: PSMA PET/CT study is a very sensitive test in detection of recurrent prostate cancer. Despite definitive surgical treatment to the prostate gland, this study demonstrated that as high as 76.7% of our patient population showed recurrence in the prostate bed, as well as regional and distant metastasis. For the patients with rising PSA and higher Gleason scores, especially those at a higher risk, we recommend PSMA PET/CT to evaluate the recurrence and extent of the disease for a better treatment strategy.

POSTER #27

Title: Diagnosis, Please! Test Your Radiologic Reasoning

Authors: Veronica Pereira, M.D., Muhammad Awais Ashraf, D.O., Prasanta Karak, M.D.
Affiliation: Department of Radiology, Hartford Hospital, Hartford, CT

Background:
Breast cancer remains the most frequently diagnosed malignancy and the second leading cause of cancer-related mortality among women in the United States, with over 310,000 new invasive cases and 42,000 deaths expected in 2025[1]. Roughly 80% are hormone receptor (HR)-positive, defined by estrogen (ER) and/or progesterone receptor (PR) expression[2].

Determining receptor status is fundamental to prognosis and treatment selection, guiding endocrine and targeted therapies such as aromatase inhibitors, SERDs, or CDK4/6 inhibitors. Cerianna (fluoroestradiol F-18, FES) is an FDA-approved PET radiotracer that binds specifically to the estrogen receptor, enabling noninvasive whole-body imaging of ER expression[3]. This imaging modality provides a "functional receptor map" that complements tissue-based testing and allows for visualization of receptor activity across the entire extent of disease[4].

Methods:
This case report describes the use of ^{18}F-fluoroestradiol (Cerianna) PET/CT performed for restaging in a patient with stage IV breast cancer with established osseous metastases. Standard whole-body PET/CT was acquired following intravenous administration of the FES radiotracer.

Case Description/Results:
A 65-year-old woman with invasive lobular carcinoma of the left breast, initially treated with lumpectomy, radiotherapy, and five years of anastrozole (2015–2020), presented with recurrent, diffusely metastatic disease in 2022 and began exemestane plus abemaciclib in 2023. A restaging bone scan on August 15, 2025, showed extensive multifocal skeletal uptake, suspicious for disease progression compared with April 2025. To differentiate progression from treatment-related effects, a Cerianna PET/CT was obtained.

The study demonstrated diffuse, symmetric, intense skeletal tracer uptake involving the vertebrae, pelvis, ribs, and proximal long bones, creating a "superscan" pattern. The extent and uniformity of uptake can be misleading, as it may resemble the distribution seen with other PET tracers such as FDG, rather than the typically focal pattern of Cerianna.

To establish the diagnosis, it's essential to **reason through the imaging findings step by step**:

1. Consider **what radiotracer was used**. The absence of radiotracer uptake in the brain excludes FDG. The absence of uptake in the salivary and lacrimal glands excludes PSMA tracers, while non-visualization of the pituitary, thyroid and adrenal glands rules out DOTATATE tracers. Finally, the visualization of the gallbladder in combination with non-visualization of brain parenchyma confirms the use of Cerianna as the PET tracer.

2. **What's the diagnosis?** Taken together, these findings confirm widespread ER-positive metastatic disease, consistent with a high skeletal tumor burden and advanced-stage progression.

Conclusions:

This case illustrates the unique yet potentially misleading appearance of a Cerianna "superscan," characterized by diffuse, intense skeletal uptake reflecting widespread ER-positive metastatic disease. Recognizing this pattern can be challenging, as it may resemble other tracer distributions; however, applying a systematic approach when evaluating the physiologic distribution of the PET tracer cinches the diagnosis. Ultimately, accurate identification of this imaging pattern is essential for correct interpretation and treatment planning, ensuring appropriate continuation of endocrine therapy, or, conversely, recognizing true disease progression when present.

References:

[1.] American Cancer Society. (2025). *Cancer Facts & Figures 2025.* Atlanta, GA: American Cancer Society. https://www.cancer.org/research/cancer-facts-statistics.html

[2.] Fowler, A. M., Mankoff, D. A., & Linden, H. M. (2022). Molecular imaging of breast cancer: FDG PET and beyond. *Radiographics*, 42(4), 1090–1113. https://pubs.rsna.org/doi/full/10.1148/rg.220143

[3.] U.S. Food and Drug Administration. (2020). *Cerianna (Fluoroestradiol F-18) Injection – Prescribing Information.* Silver Spring, MD: U.S. Food and Drug Administration. https://www.accessdata.fda.gov/drugsatfda_docs/label/2020/212155s000lbl.pdf

[4.] Linden, H. M., Peterson, L. M., & Mankoff, D. A. (2018). Estrogen receptor imaging and dynamics with FES PET. *PET Clinics*, 13(3), 415–422. https://doi.org/10.1016/j.cpet.2018.02.005

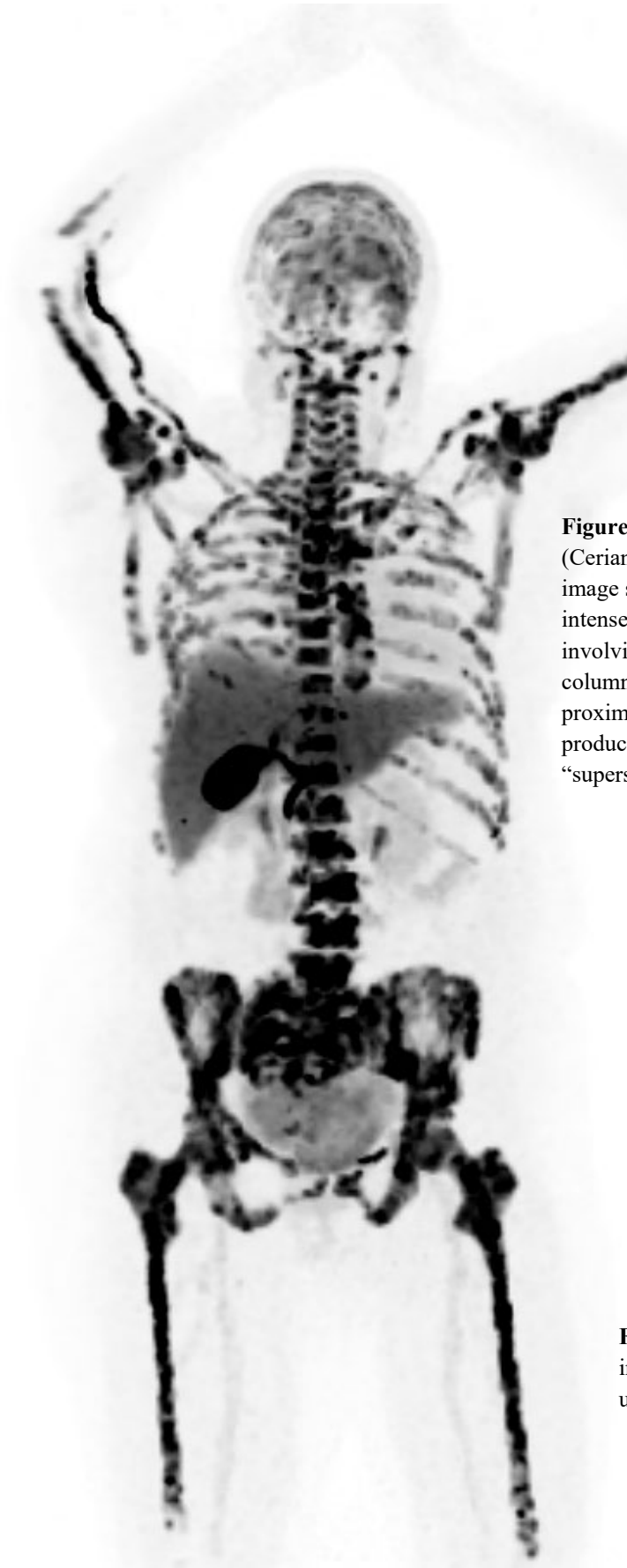

Figure 1. ^{18}F-fluoroestradiol (Cerianna) PET/CT MIP image shows diffuse and intense radiotracer uptake involving the vertebral column, pelvis, ribs and proximal long bones, producing the appearance of a "superscan."

Figure 2. Coronal fused PET image from the same index patient highlighting the absence of tracer uptake within the brain and submandibular glands.

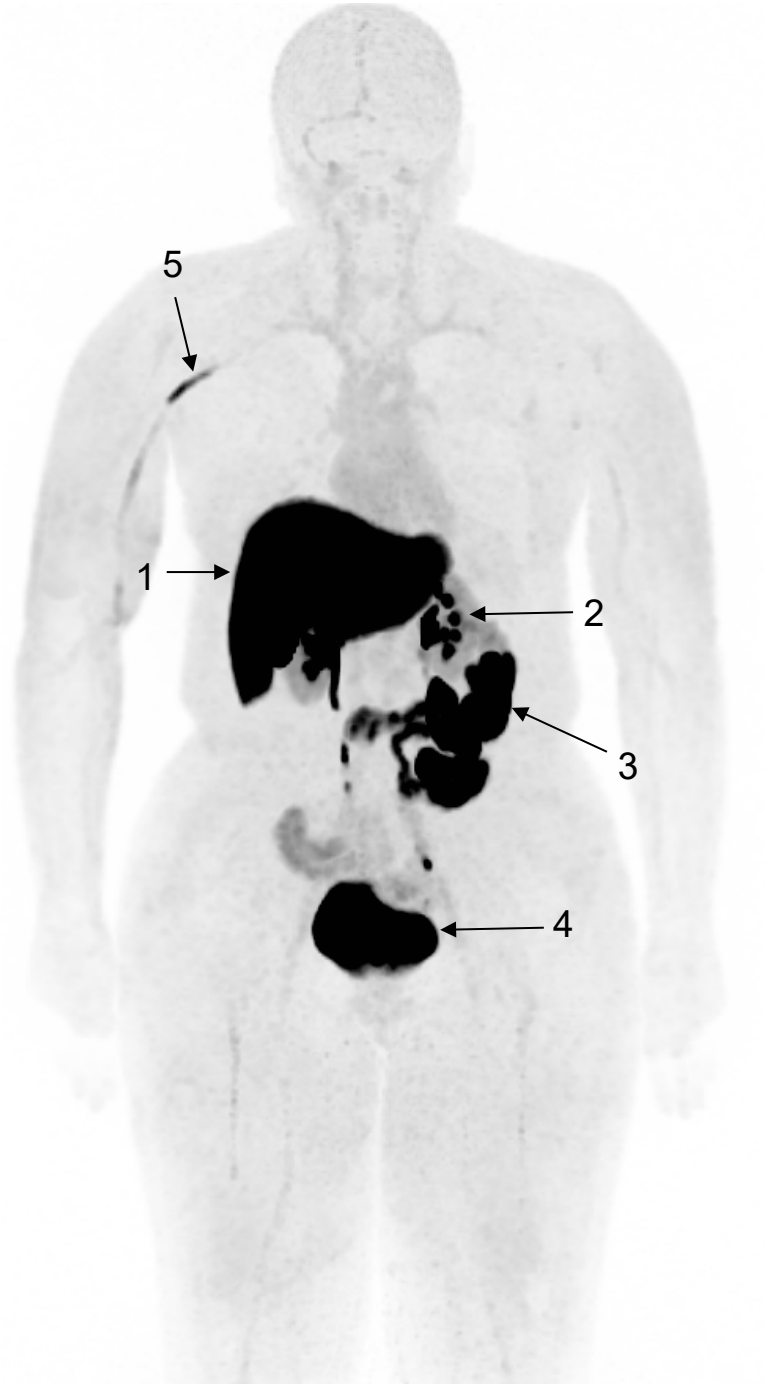

Figure 3: This MIP image shows the physiologic distribution of fluoroestradiol F18 during PET scan, with accumulation in the liver (1), and extraction by the kidneys (2), GI tract (3) and urinary bladder (4). Tracer uptake can also be seen in the injected vessel (5).

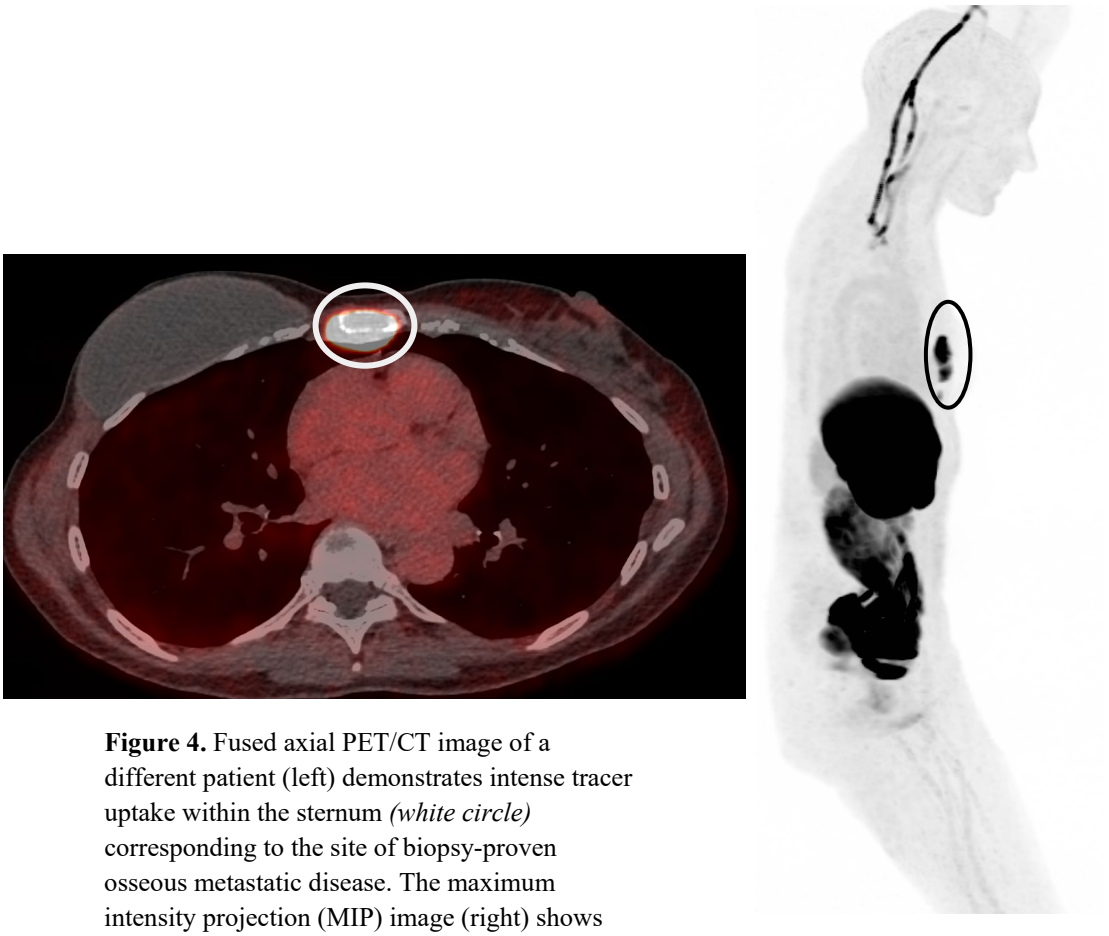

Figure 4. Fused axial PET/CT image of a different patient (left) demonstrates intense tracer uptake within the sternum *(white circle)* corresponding to the site of biopsy-proven osseous metastatic disease. The maximum intensity projection (MIP) image (right) shows this lesion *(black circle)*.

Figure 5. MIP image of a different patient shows a dominant confluent FES-avid right axillary soft tissue mass at the site of a biopsy-proven metastatic lymph node (1) and additional right subpectoral tracer-avid lymph node (2).

POSTER #28